



## OPEN ACCESS

## EDITED BY

Kwon Rausis,  
BluMetric Environmental Inc., Canada

## REVIEWED BY

Davide Ciceri,  
Agroplantae, United States  
Ingrid Smet,  
Independent researcher, Fuerth, Germany  
Salvatore Calabrese,  
Texas A&M University, United States

## \*CORRESPONDENCE

Nicholas Iff  
✉ nicholas.iff@fu-berlin.de

RECEIVED 03 July 2023

ACCEPTED 12 April 2024

PUBLISHED 30 April 2024

## CITATION

Iff N, Renforth P and Pogge von Strandmann PAE (2024) The dissolution of olivine added to soil at 32°C: the fate of weathering products and its implications for enhanced weathering at different temperatures. *Front. Clim.* 6:1252210.  
doi: 10.3389/fclim.2024.1252210

## COPYRIGHT

© 2024 Iff, Renforth and Pogge von Strandmann. This is an open-access article distributed under the terms of the [Creative Commons Attribution License \(CC BY\)](#). The use, distribution or reproduction in other forums is permitted, provided the original author(s) and the copyright owner(s) are credited and that the original publication in this journal is cited, in accordance with accepted academic practice. No use, distribution or reproduction is permitted which does not comply with these terms.

# The dissolution of olivine added to soil at 32°C: the fate of weathering products and its implications for enhanced weathering at different temperatures

Nicholas Iff<sup>1\*</sup>, Phil Renforth<sup>2</sup> and Philip A. E. Pogge von Strandmann<sup>3</sup>

<sup>1</sup>Mainz Isotope and Geochemistry Centre (MIGHTY), Institute of Geosciences, Johannes Gutenberg University, Mainz, Germany, <sup>2</sup>The Research Centre for Carbon Solutions, Heriot-Watt University, Edinburgh, United Kingdom, <sup>3</sup>London Geochemistry and Isotope Centre (LOGIC), Department of Earth Sciences, University College London, London, United Kingdom

The amendment of agricultural soils by crushed silicate minerals has been proposed to enhance weathering rates and facilitate carbon dioxide (CO<sub>2</sub>) removal from the atmosphere. Laboratory dissolution experiments typically provide weathering rates that are significantly higher than those observed under natural conditions, while field studies are limited in the nature of data they can collect. This study uses an experimental setup that aims to emulate natural field conditions in a controlled setting using soil cores retrieved from UK cropland amended with crushed olivine at 32°C. Results are compared to enhanced weathering experiments run at 4°C and 19°C under otherwise identical conditions. The data reveal temperature-dependent variations in the behaviour of different elements, most importantly Mg and Si, with silicon being retained at moderate temperatures and magnesium being retained at higher temperatures. These patterns are most likely due to different retention mechanisms, notably Si reprecipitation (e.g. as cation-depleted Si-enriched mineral surface coatings) and cation exchange (affecting Mg, but to a lesser degree Si), such that the influence of cation exchange should be accounted for when interpreting enhanced weathering field data. We therefore recommend that estimates of carbon sequestration should not be based on the behaviour of individual elements. A temperature effect on the weathering rate of olivine added to soil columns is observed with the weathering rate being higher at 32°C than at 19°C and 4°C, and significantly lower than laboratory experiment-derived weathering rates. This further emphasises the need for enhanced weathering field trials, as simple laboratory-derived rates cannot be used to assess the feasibility of enhanced weathering measures. The carbon dioxide capture potential at 32°C is conservatively estimated at ~115 t CO<sub>2</sub> km<sup>-2</sup> yr<sup>-1</sup> assuming an olivine amendment rate of 12.7 kg m<sup>-2</sup>. Our data suggests that soil accumulation of heavy metals like Cu and Cr at high temperatures (hence high weathering rates) is non-dangerous, however, Ni concentrations in the effluent solution are close to EU guidelines while Cr and Cu are considerably lower than guidelines. All of these conclusions have implications for the application of enhanced weathering for carbon dioxide removal from the atmosphere.

## KEYWORDS

olivine dissolution, weathering experiment, carbon sequestration, carbon dioxide removal (CDR), enhanced weathering, temperature effect on weathering, cation exchange, negative emission technologies (NET)

## Introduction

Anthropogenic carbon dioxide ( $\text{CO}_2$ ) emissions are leading to an increase in temperatures due to the greenhouse effect. Current predictions clearly show that if emissions remain constant, global temperatures will rise  $1.5^\circ\text{C}$  within just the next two decades (IPCC, 2021). Reduction of  $\text{CO}_2$  emissions is no longer sufficient to meet climate goals that were agreed upon in the 2015 Paris Agreement (UNFCCC, 2015). In addition to deep emission reduction, the rapid development and deployment of carbon dioxide removal (CDR) has been proposed as a measure to avoid the climate crisis. 100–1,000 Gt $\text{CO}_2$  need be removed from the atmosphere by 2100 to restrict global warming to  $2^\circ\text{C}$  (Psarras et al., 2017; Rockström et al., 2017; IPCC, 2022).

On geological timescales, the consumption of  $\text{CO}_2$  through silicate weathering plays the primary role in regulating Earth's atmospheric  $\text{CO}_2$  concentrations (Walker et al., 1981; Saenger and Wang, 2014), and accounts for ~65% of total global chemical weathering. Here, the basalt weathering proportion of silicate rock weathering amounts from 16.5% (Hartmann et al., 2009) to 35% (Dessert et al., 2003), although basalt covers only ~5% of the land surface, as it is more susceptible to weathering in comparison to, e.g., felsic rocks such as granite (Suchet and Probst, 1995). The weathering of silicate rocks releases base cations and generates alkalinity. Weathering products are subsequently transported to the oceans via continental runoff (Meybeck, 1987), where they increase ocean alkalinity, which causes an increased net  $\text{CO}_2$  flux into the oceans (Renforth and Henderson, 2017). Eventually, those weathering products (e.g., bicarbonate, calcium) are locked away in carbonate deposits after having been biogenically bound during shell formation of marine organisms (Kasting, 2019). At present natural conditions, the rate of chemical silicate weathering is slow at ~0.26 GtC  $\text{y}^{-1}$  (equivalent of ~1 Gt $\text{CO}_2$   $\text{yr}^{-1}$ ; Hartmann et al., 2009). Silicate weathering is primarily limited by supply of primary silicates and climate-related factors (runoff, temperature etc.; Raymo and Ruddiman, 1992; Berner, 2003; West et al., 2005). Enhanced weathering (EW) aims at increasing the availability of fresh, weatherable materials by spreading silicate minerals on land (Schuiling and Krijgsman, 2006; Köhler et al., 2010; Renforth, 2012; Hartmann et al., 2013; Taylor et al., 2016), coasts (Hangx and Spiers, 2009; Schuiling and de Boer, 2010), or the ocean (Renforth et al., 2013) and increasing the weatherable surface of the respective minerals or rocks by comminution. Theoretically, smaller grain sizes lead to higher dissolution rates; however, additional  $\text{CO}_2$  emissions may be created by the comminution of rock to such grain sizes, which is why the quantification of the dissolution and thus sequestration rate is necessary (Renforth, 2012). Enhanced weathering is expected to be more effective in (sub-)tropical regions with high temperatures and precipitation (Hartmann et al., 2013; Taylor et al., 2016; Strelfer et al., 2018). It is hence important to identify processes, e.g., in the soil, that

may influence the dissolution of silicates and the transport of weathering products under such conditions, and whether those processes exhibit temperature-dependent behaviour. Yet, those complex soil processes that influence weathering are difficult to elucidate. For example, the formation of secondary encapsulating and passivating silica-rich amorphous layers was found to have a limiting effect on weathering (Béarat et al., 2006; Rigopoulos et al., 2018; Amann et al., 2020; Fuhr et al., 2022) and the effect of cation exchange in the context of terrestrial enhanced weathering (EW) measures, which represent conditions that are not typically found in nature, is uncertain. For example, the timescale of enhanced rock weathering is multiple orders of magnitude shorter compared to the naturally occurring silicate rock weathering, which has been more thoroughly studied in previous research, but tends to already be at some semblance of steady-state. These very rapid timescales could lead to other processes becoming important in this context, which do not play a significant role over the longer periods of time on which natural weathering operates. Weathering rates derived from laboratory studies are generally much higher than the rates determined from catchment-scale measurements (White and Brantley, 2003), and the dissolution rates of artificially added silicates have received less attention (Peters et al., 2004; ten Berge et al., 2012; Manning et al., 2013; Renforth et al., 2015). Renforth et al. (2015) used soil columns extracted from an agricultural field and operated as lysimeters in the laboratory at  $19^\circ\text{C}$ . This design maintains some of the complexity of soil processes, while being able to control material inputs and outputs, as well as additional factors such as temperature and precipitation. Pogge von Strandmann et al. (2022) later reproduced the experiment at  $4^\circ\text{C}$ . Our experiment is likewise carried out in the same manner using soil cores extracted from the same site at the same time, but now at  $32^\circ\text{C}$ , with the aim of drawing conclusions on how temperature controls the global spatial application of olivine powder as an EW technology, and furthermore to constrain whether soil behaviour changes with temperature. Moreover, in the context of EW approaches, heavy metal pollution (Ni, Cr, Cu) from the amendment rock constitutes one major limitation and is thus important to assess, especially as the expected faster silicate weathering rates at higher temperatures should equally lead to a faster release of soil contaminants. The release of toxic heavy metals is hence investigated to determine whether the amendment of agricultural lands with olivine in warm climates might entail inadvertent hazardous side effects (Haque et al., 2020).

## Experimental design

Renforth et al. (2015) extracted soil cores measuring 1 m in length and 10 cm in width from an agriculturally used land in North Oxfordshire, mounted those cores as lysimeters in a  $19^\circ\text{C}$  temperature-controlled laboratory and amended with 100 g powdered olivine. The calcareous soil cores encompass the ploughed layer on top, B and C

horizons and parent rock at the bottom, which is constituted of fossiliferous Jurassic bioclastic oolitic limestone (the uppermost Cornbrash Formation; Powell and Riding, 2016). One core was used to determine bulk soil compositions and leachable phases (exchangeable fraction, carbonates) by means of XRF and mass spectrometry, as well as TOC (total organic carbon) and TIC (total inorganic carbon) contents through coulometric carbon analyses. These reveal for example the presence of carbonates (through both direct analyses and sequential leaching), while the presence of clays and quartz is demonstrated by the residual composition after leaching. Furthermore, XRD analyses of the post-treatment control column show that the soil is mainly composed of quartz in the upper parts of the column and calcite in the lower parts of the column, while the abundances of muscovite (likely secondary), feldspars and clays are generally very low (Supplementary Table 1). Mg and Li isotope analyses are reported by Pogge von Strandmann et al. (2021) where the latter demonstrate the impact of the exchangeable fraction on cation retardation at 19°C, with a potential smaller component of secondary mineral formation as well. Renforth et al. (2015) amended olivine from Western Norway (Minelco Ltd.). The same olivine was used in the 4°C experiment (Pogge von Strandmann et al., 2022) and in this experiment at 32°C. This olivine powder was analysed for its elemental composition, grain size and surface area using XRF, dry sieving and BET surface area analyses, respectively (Supplementary Table 2).

In this experiment, two of the cores were set up in a darkened room to prevent algal growth in solution containers. The room was heated to 32°C and the experiment conducted in the same way as the previous experiments at lower temperatures (Figure 1). Besides the identification of the influence of temperature on soil behaviour, this study also aims to evaluate the effectiveness of enhanced weathering in hot, tropical conditions. In this context, it is important to note that tropical and temperate soils exhibit distinct characteristics shaped by their respective climates. For example, soils in temperate regions tend to have a higher organic matter content due to slower decomposition rates. This provides, e.g., binding sites for cation exchange. Conversely, tropical soils, subjected to warmer and more humid conditions,

experience rapid organic matter breakdown, generally resulting in lower organic content (Brady and Weil, 2016).

A modified Hoagland solution, mimicking rain water and fertiliser (Supplementary Table 3), was dripped onto the top of the columns at a constant high rate of 15 mL/h for 40 days to allow for habituation of the soil exchange complex towards the disequilibrium caused by the sudden addition of Hoagland solution. Note that the solution we used contained Na, while the solution used by Renforth et al. (2015) and Pogge von Strandmann et al. (2022) did not. To one of the columns, we added 29.43 g (which equals ~3.7 kg/m<sup>2</sup>) of olivine powder to the top 20 cm, which were thoroughly mixed, while the other core was also stirred but no olivine was added and was used as control column. In comparison, the highest proposed rate in modelling studies is 5 kg/m<sup>2</sup> (Taylor et al., 2016) to 15 kg/m<sup>2</sup> (Strefler et al., 2018). Effluent solutions were periodically collected at the base of each core. The experiment was terminated after 79 days as the olivine-treated column became impermeable, likely due to the swelling of clays at the relatively high temperatures, possibly combined with a barrier formed partway down the core by pieces of bedrock.

## Methods

Soil samples were extracted from both cores in 10 cm increments after the experiment. We subsequently applied two steps of a sequential leaching sequence to the soils of both the experimental and control column to extract the exchangeable (in 1 M sodium acetate, pH = 8) and the carbonate (in 1 M Acetic Acid, pH = 5) fractions, respectively (Tessier et al., 1979). These can then be compared to identical sequential extractions of the pre-reaction core and post-reaction core of the 19°C experiment (Renforth et al., 2015).

The effluent solutions, exchangeable fractions and carbonate fractions were analysed for their major and minor elemental concentrations using a Triple Quadrupole 8900 ICP-MS (Agilent Technologies) at Johannes Gutenberg University, Mainz, with calibration curves comprised of multi-element standards. SLRS-6 (National Research Council of Canada) was used as a reference material. Long-term analytical reproducibility on this instrument is better than ±5%. Less olivine was added to the column in this experiment at 32°C than in the lower temperature studies (29.432 g vs. 100 g). We use a scaling factor of ~3.398 to  $\Delta X_{\text{olivine-control}}$  in order to be able to directly compare the results of our study with those of the previous studies conducted at 4°C (Pogge von Strandmann et al., 2022) and 19°C (Renforth et al., 2015) due to lower application rates in this study (29.43 g) than in the lower temperature studies (100 g). Here,  $\Delta X_{\text{olivine-control}}$  denotes the difference between the olivine-treated column's and control column's concentrations of the respective measured element. This however introduces a level of uncertainty, as the different olivine:matrix ratios could lead to varying saturation states with respect to a variety of minerals. We thus used PHREEQC v3 (Parkhurst and Appelo, 2013; llnl.dat database) to investigate the saturation states of various solid phases in the effluent solution samples (Supplementary Table 4). Element concentrations of the exchangeable and carbonate fractions obtained through sequential leaching are given in Supplementary Table 5. All measurements were well above limit of detection. For XRD measurements, 3 g of preground samples were micronised with 20 mL of cyclohexane in an XRD-Mill McCrone (RETSCH) equipped with a set of agate elements. The mixture was ground for 7 min to a grain size of <10 µm. Cyclohexane was then evaporated in air. X-ray powder diffraction (XRPD) was

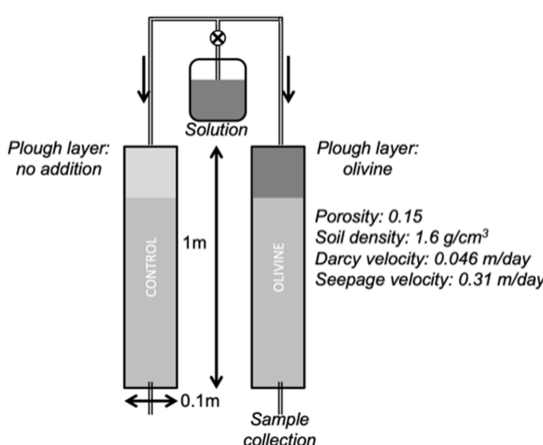


**FIGURE 1**  
Schematic of the experimental setup (modified after Renforth et al., 2015; Pogge von Strandmann et al., 2022).

recorded using a Seifert XRD 3000 TT with Cu K $\alpha$  radiation (40kV, 30mA) in Bragg–Brentano configuration (automatic divergence slit, irradiated sample width: 10 mm). Each sample was scanned over the measuring range 5–60° 2 $\theta$  at an angular rate of 0.03° 2 $\theta$ /s and a dwell time of 5 s/step. Phases were identified and quantified using the Profex (Doebelin and Kleeberg, 2015) software with the Rietveld refinement.

## Results

Over the course of the experiment, ~32 L of Hoagland solution was drip-fed through the columns. The effluent solution pH values of both columns increased because of the consumption of protons during weathering processes. The increase is more pronounced in the olivine-treated column after an initial drop (Figure 2). Such lowered pH during the first days of the experiment is due to olivine-derived cations exchanging with protons on negatively charged surface sites in the soil, which are then released to solution. After day ~30, the pH of the olivine-treated column's effluent solution increases more strongly than that of the control column, possibly because the majority of the previously adsorbed H $^+$  was released and the pH increase due to olivine weathering becomes noticeable.

### Major elements (Mg, Ca, Si)

Figure 3 shows the time series of the major and trace element concentrations of the effluent solution. The data was corrected for input through the Hoagland solution. Detailed Hoagland solution concentrations and concentrations of the effluent solution are reported in Supplementary Table 3. After 23 days, magnesium concentrations (Figure 3A) of the olivine-treated column (2.17  $\mu\text{gg}^{-1}$ ), become lower than from the control column (2.29  $\mu\text{gg}^{-1}$ ) and decrease continuously.

Meanwhile control column Mg concentrations increase until day 58 (2.47  $\mu\text{gg}^{-1}$ ), after which they decrease rapidly. Ca concentrations of both columns show a general decreasing trend, while control column values are higher than those of the olivine-treated column (Figure 3B). Until day 28, [Si]<sub>ol</sub> and [Si]<sub>ctl</sub> are not resolvably different. [Si]<sub>ol</sub> exceeds [Si]<sub>ctl</sub> after day 28 and exhibits an increasing trend until the end of the experiment (max. ol concentration 8.03  $\mu\text{gg}^{-1}$ , max. Ctl concentration 4.71  $\mu\text{gg}^{-1}$ ), while control column concentrations increase only marginally (ol final solution 6.82  $\mu\text{gg}^{-1}$ , ctl final solution 4.24  $\mu\text{gg}^{-1}$ ; Figure 3C).

### Trace elements

Effluent Cr concentrations (Figure 3D) of both columns started at about 0.40 ng/g and after an initial increase gradually decreased towards zero by the end of the experiment. Apart from elevated spikes in the control effluent at the start and towards the end of the experiment, the olivine treated column had higher Cr concentrations than the control. At the end of the experiment both treatments approach zero. Ni concentrations (Figure 3E) of the olivine-treated column are on average higher than those of the untreated column, and show an increasing trend after a spike on day 4 (3.30 ng/g), while control column Ni concentrations stay similar throughout the course of the experiment (~0.25 ng/g) after an initial spike on day 9 (2.35  $\mu\text{g}/\text{g}$ ). Towards the end of the experiment, olivine-treated and control column values exhibit the maximum difference on day 74 (ol 1.81  $\text{ng g}^{-1}$ , ctl 0.32  $\text{ng g}^{-1}$ ). Cu (Figure 3F) likewise shows strong fluctuations during the early experimental stages. Afterwards, [Cu]<sub>ol</sub> is continuously higher than [Cu]<sub>ctl</sub> and effluent solution concentrations of both columns increase (final ol 5.03  $\text{ng g}^{-1}$ , ctl 2.26  $\text{ng g}^{-1}$ ).

### Geochemical modelling (PHREEQC)

All effluent solutions are undersaturated with respect to olivine (forsterite) and oversaturated with respect to clay minerals (kaolinite, beidellite, montmorillonite; Figure 4). During the course of the experiment, the saturation indices (SI) of both forsterite and clays in the olivine-treated column increase relative to those of the control column. This can likely be attributed to the increase in pH (Figure 2). For instance, SI of forsterite in the olivine-treated column are highly correlated with pH ( $r=0.99, n=19$ ). For clays, the additional input of olivine-derived weathering products could further contribute to higher SI. Importantly, the SI values are very similar to those at 19°C (Renforth et al., 2015) and indicate that it is possible to compare the experiments, although the absolute amounts of added olivine are less.

### XRD

Integrating over the whole column, calcite (43.27%) and quartz (39.97%) are the most abundant minerals. Muscovite (5.44%) and clays (illite, kaolinite, montmorillonite; 4.97%) are minor constituents of the column. Feldspar (anorthoclase, oligoclase, orthoclase) contents too are low at 4.65%, as well as pseudorutile (1.13%) and goethite (0.57%). Quartz abundance is highest in the uppermost parts of the column and decreases with depth. The opposite is observed for calcite, which is the major constituent in the lower parts of the soil column as the parent rock is oolithic limestone (Supplementary Table 1).

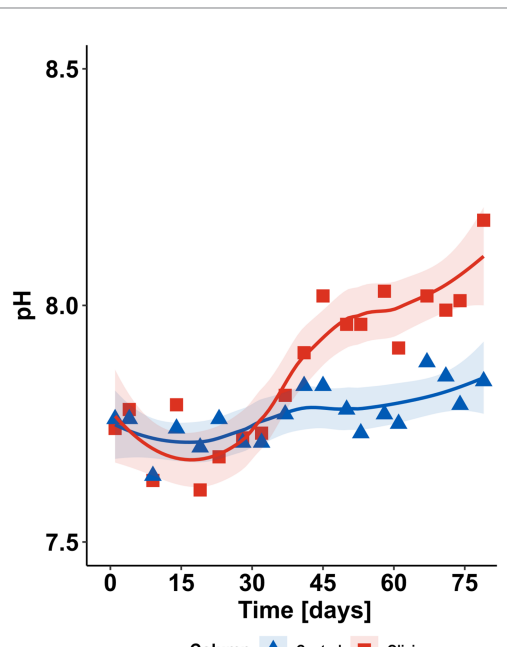
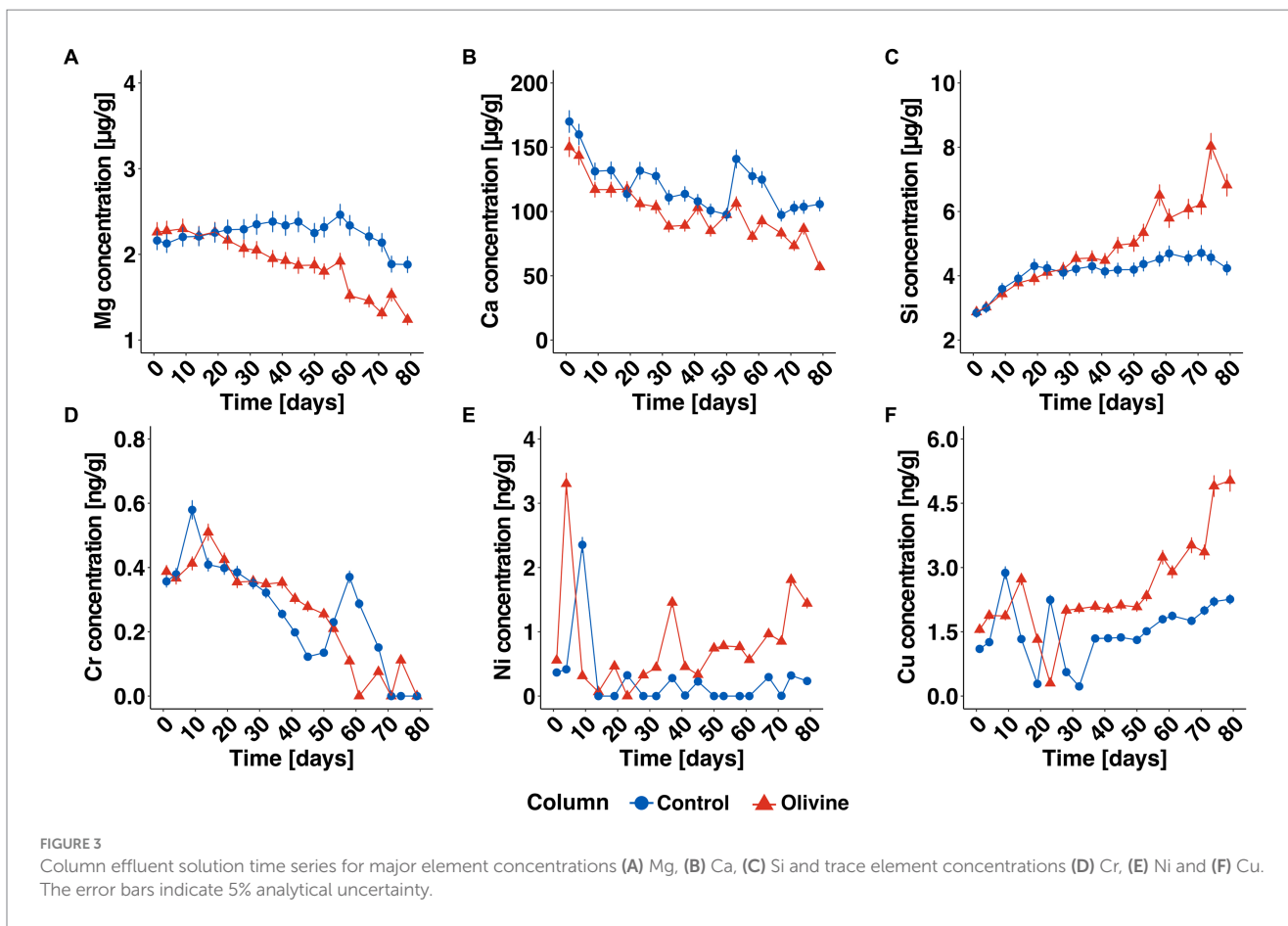


FIGURE 2  
Time series of pH in the effluent solutions of both control and olivine-treated columns. The shaded areas indicate 1SE.



## Discussion

In the columns, three materials can dissolve and release ions – existing soil carbonates, existing soil silicates and in the olivine-treated column, the added forsterite. The amended olivine is hence assumed to be the only difference in possible cation source between the experimental and control core, as we expect minimal inhomogeneities of the soil, given that the cores were extracted within a few metres of each other. Note that the elemental values of the effluent solutions represent net values, as the weathering products can have different fates, meaning that the measured element concentrations might be influenced by consumption during secondary mineral formation, by sorption processes in the soil (Renforth et al., 2015; Pogge von Strandmann et al., 2021, 2022), or by stabilisation of soil organic matter (SOM) through physicochemical protection mechanisms (Song et al., 2018; Calabrese et al., 2022).

## The sources of Mg

### Relationship between magnesium and silicon

Figure 5A displays the relationship between silicon and magnesium concentrations in the effluent solutions. We observe a negative covariation between Mg and Si in the olivine-treated column—hence, Mg concentrations are lower when Si concentrations, indicative of olivine dissolution, are higher. This is unexpected, as the added forsterite ( $\text{Mg}_2\text{SiO}_4$ ) is rich in both Mg and Si. In contrast, at

19°C, the Si-Mg relationship was positive, and the control and olivine-treated columns demonstrated a similar slope, while at the same time, the olivine core's effluent solution was more enriched in Mg due to additional input of the added olivine and shifted towards more positive values (Renforth et al., 2015). In contrast, the Mg in the effluent solution in this experiment cannot be conclusively attributed to olivine dissolution. In the control column, Mg and Si do not covary, which implies that Mg is only marginally sourced from the dissolution of pre-existing silicates.

Furthermore, at 32°C more Si leaves the control column, to which we did not add olivine (average [Si] 4.14 µg/g) than at 19°C (average [Si] 1.78 µg/g) and 4°C (1.12 µg/g). Possible explanations are that higher temperatures result in higher breakdown of primary and/or secondary silicates, as also observed during natural weathering (Gislason et al., 1996; Stefansson, 2001; Pogge von Strandmann et al., 2017), or Si is preferentially retained through secondary processes at moderate temperatures.

### Relationship between magnesium and calcium

Figure 5B illustrates the covariation between calcium (Ca) and magnesium (Mg) concentrations in the effluent solutions. These elements exhibit a co-variation coming from the olivine-treated column, implying a common source, most likely attributed to dissolving carbonates present in the soil. Conversely, in the control column, no discernible co-variation is observed. Furthermore, neither the effluent of the olivine-treated nor the control column exhibit a

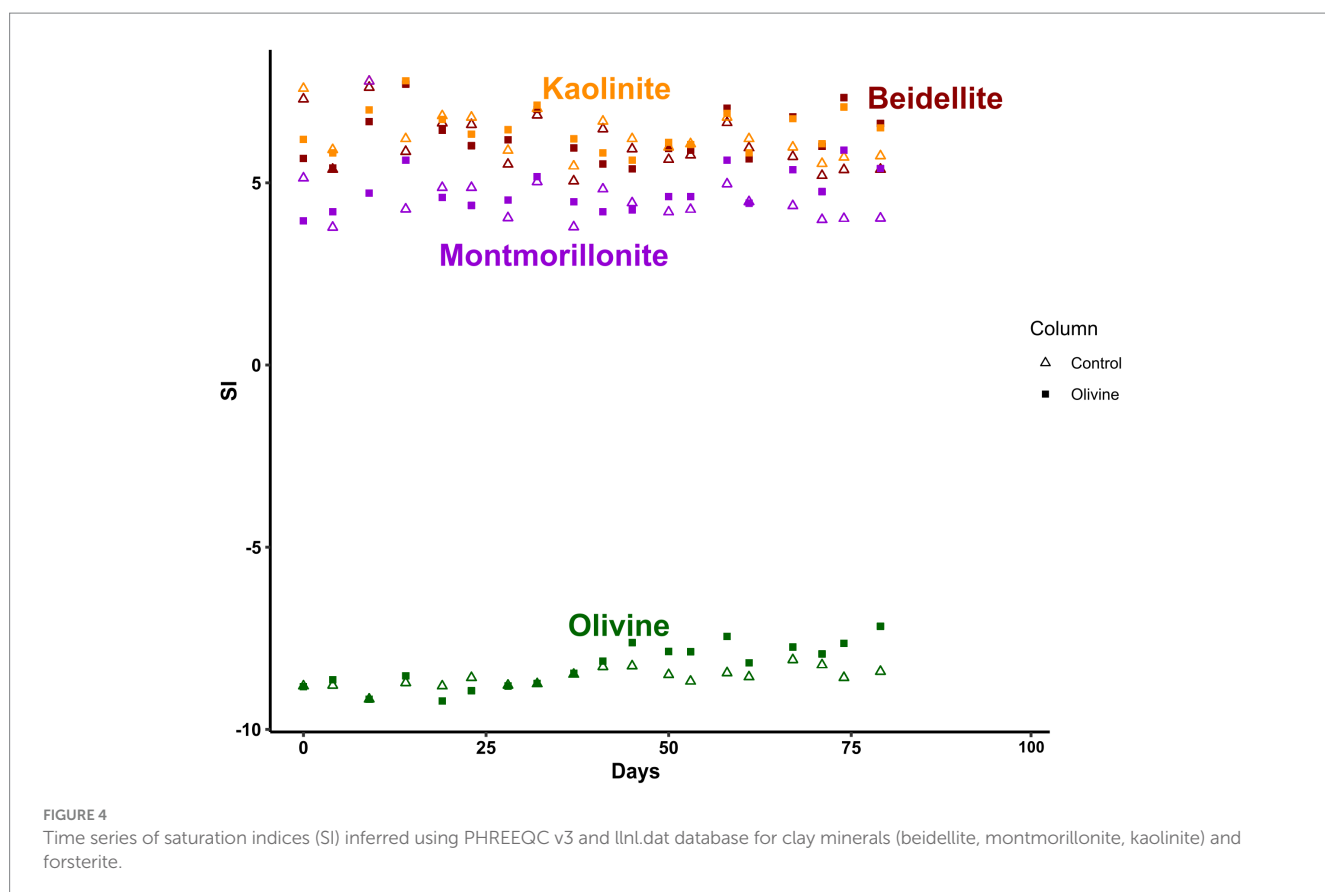


**FIGURE 4**  
Time series of saturation indices (SI) inferred using PHREEQC v3 and llnl.dat database for clay minerals (beidellite, montmorillonite, kaolinite) and forsterite.

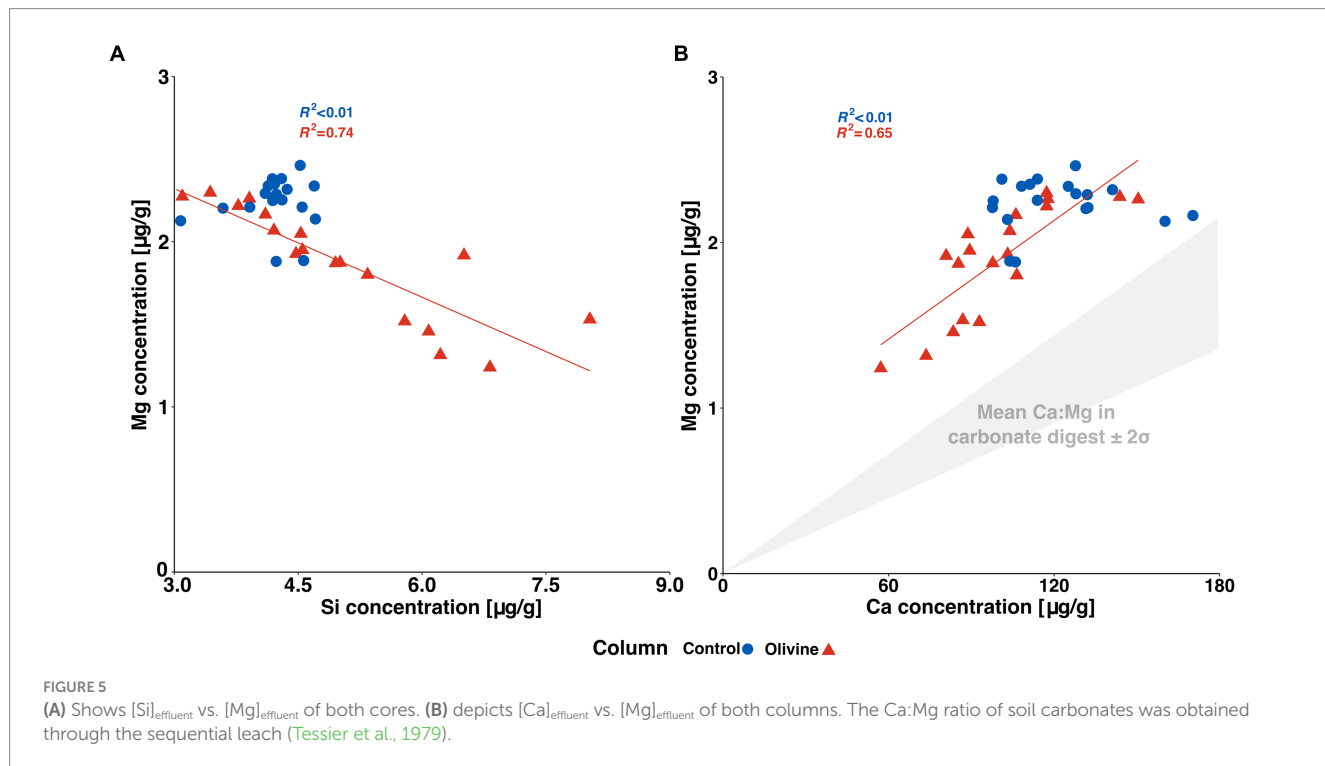


**FIGURE 5**  
**(A)** Shows  $[Si]_{\text{effluent}}$  vs.  $[Mg]_{\text{effluent}}$  of both cores. **(B)** depicts  $[Ca]_{\text{effluent}}$  vs.  $[Mg]_{\text{effluent}}$  of both columns. The Ca:Mg ratio of soil carbonates was obtained through the sequential leach (Tessier et al., 1979).

similar Ca:Mg ratio to the soil carbonates. It is thus reasonable to conclude that the similar behaviour in the olivine-treated column is not solely due to the dissolution of carbonates, but that further Mg is

sourced from an additional reservoir. This leaves the exchangeable fraction as a prime candidate, which might act both as a cation source and cation sink through adsorption–desorption processes.

## Magnesium mass balance of the control column shows the significant role of cation exchange

Based on several assumptions, a mass balance of the Mg output can be established. Note that it was not possible to draw up the mass balance for the olivine-treated column because the concentrations of magnesium in the effluent are lower than in the control column. This would lead to negative values due to the assumptions made hereafter, and implies that the olivine-derived Mg may not reach the effluent solution. This is further discussed below. The first assumption is that the input-corrected Ca flux from the control column originates from the dissolution of carbonates, as demonstrated by Renforth et al. (2015), who found a linear correlation between the Ca concentration and the total inorganic carbon (TIC) in the solid phase of the cores. Given our discussion below about the influence of the exchangeable pool, and that Ca and Mg are similarly mobile (within a factor of 2–3) during weathering (e.g., Gislason et al., 1996; Pogge von Strandmann et al., 2016), some Ca may also stem from the exchangeable pool, and hence cause us to overestimate carbonate dissolution. However, especially in a carbonate-dominated core, this is unlikely to be by a significant amount, and, for example, Tipper et al. (2021) estimate that 5% of total particle-borne Ca is in the exchangeable fraction. The second assumption is that the input-corrected effluent Si flux from the control core can be ascribed to dissolution of already existing silicates. The abundance of quartz is assumed to have no effect on the chemical composition of the effluent waters due to its very high weathering resistance. The measured mean Mg/Ca and Mg/Si ratios of the leached carbonate fraction and initial bulk material, respectively, are subsequently used to determine the proportion that each phase contributes to the material leaving the core in the effluent solution. The Mg remaining after correction for pre-existing silicate and carbonate dissolution is assumed to derive from the exchangeable fraction, i.e., through desorption from negatively charged surface sites. In theory, if this mass balance was performed for the olivine-treated core, the effluent values unexplained by the dissolution of carbonates, silicates and the exchangeable fraction would represent Mg that is derived from the dissolution of olivine. The influent solution did not contain Mg. The mass balance equation is thus:

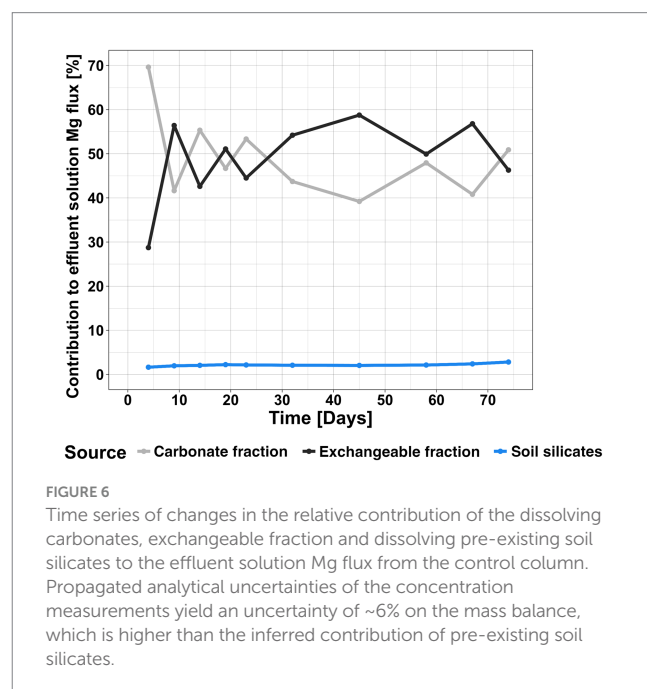
$$Mg_{exch} = Mg - \left[ \left( \frac{Mg}{Ca} \right)_{carb} \times Ca \right] - \left[ \left( \frac{Mg}{Si} \right)_{bulk} \times Si \right] \quad (1)$$

$Mg_{exch}$  is that part of the effluent Mg that is sourced from the cation exchange complex, Mg the magnesium flux from the column,  $(Mg/Ca)_{carb}$  the ratio between magnesium and calcium in the carbonate fraction obtained through the sequential leach and calcium the flux of calcium from the core,  $(Mg/Si)_{bulk}$  the ratio between magnesium and silicon of the initial bulk, and Si the silicon flux from the core soil (Renforth et al., 2015). The term  $[(Mg/Ca)_{carb} \times Ca]$  thus determines the amount of Mg that is sourced from dissolving carbonates and  $[(Mg/Si)_{bulk} \times Si]$  the amount of Mg coming from dissolving soil silicates.

Equation 1 was applied to mass flows of different times covering the entire experimental period to derive changes in the relative contributions of the different Mg reservoirs to the effluent solution (Figure 6). Propagated analytical uncertainties of the concentration

measurements are ~6% on the mass balance. The influence of the soil silicates remains lower than the propagated analytical uncertainty over the entire experimental period. The main Mg reservoir feeding the effluent solution at the very beginning of the experiment is the carbonate fraction, while afterwards the contribution of the carbonate and exchangeable fraction fluctuates strongly until day 23. The contribution of the exchangeable fraction subsequently increases, and in turn the relative influence of the carbonate fraction decreases. This culminates on day 45, when the exchangeable fraction contributes ~59% of the total Mg budget, while the carbonate fraction only contributes ~39%. Hence, at 32°C, the exchangeable fraction exerts higher control over Mg in the system than at lower temperatures. At 19°C, the contribution of the exchangeable fraction varied between ~44% at the start and ~32% at the end of the experiment (Pogge von Strandmann et al., 2021). At 4°C, at the end of the experiment, the exchangeable fraction contributed only ~26% to the effluent solution (Pogge von Strandmann et al., 2022). We therefore observe a positive temperature dependence of the exchangeable complex when the soil is amended with silicate powders. Nearing the end of the experiment, both values converge again. This behaviour is similar to observations made in natural systems, such as in Icelandic poorly-drained soils (used as a natural analogue of enhanced weathering, due to frequent fresh basalt addition via volcanism), where the influence of clays was higher than that of the exchangeable fraction, while in well-drained soils the exchangeable fraction exerted the higher control over the Mg behaviour (Opfergelt et al., 2014). This can however be caused by the columns becoming impermeable, which resulted in accumulation and high residence time of waters in the columns, possibly due to clay swelling. This might further hold important implications for the application of silicate mineral powders on agricultural lands at higher temperatures. Here, clay swelling may reduce water permeability and negatively impact plant growth or water drainage. Such swelling of clay minerals was not observed in the lower temperature experiments.

Note that the higher influence of cation exchange in comparison to carbonates might also be explained if carbonate dissolution



decreases – this could be the case at higher temperatures, because carbonate solubility diminishes with increasing temperature (Weyl, 1959). The average daily Ca flux from the control column is higher at 19°C (87 mg) than at 32°C (42 mg), but lower at 4°C (32 mg). However, it is unclear whether the Ca is in fact released, but retained within the core by sorption processes or secondary mineral formation, or if lower amounts of carbonates dissolve at higher temperatures due to a decrease of carbonate solubility.

## Fate of the weathering products

### Retention on the exchange complex at 32°C

The soil's cation exchange complex can, through adsorption and desorption processes, act both as a sink and a source of cations. It responds to the sudden addition of Hoagland solution, with which it is in disequilibrium, hence potentially liberating previously adsorbed cations. We introduced the 40-day pre-experimental adjustment period after observation of the 19°C experiment (Renforth et al., 2015) to counter this issue and enable the cation exchange complex to habituate to the new conditions. In theory, if this was not adequately long and the complex did not habituate at a sufficient level, an influence of the cation exchange complex is still to be expected. Equilibration can however be assumed, as Mg in solution and negatively charged surface sites have been observed to equilibrate rapidly on a timescale of hours (<4 h; Wada and Harada, 1971; Cai et al., 2022), and the average residence time of waters, based on the flow rate and measured porosity, is 3.3 days.

While in soils, Si can exist in a variety of different species ranging from monomers to oligomers and polymers, it is not clear to what proportions monosilicic and polysilicic acids, exhibiting differing sorption behaviours, were released from the dissolving olivine. Fast sorption timescales are observed for polysilicic acid (minutes), while monosilicic acid adsorbs considerably slower within weeks, as the latter exhibits a higher binding affinity than monosilicic acid (Dietzel, 2002; Schaller et al., 2021). As expected, in this experiment Si is less affected by exchange processes than cations and adsorbs in significantly lower amounts than divalent  $Mg^{2+}$ . A maximum of 7.63 µg/g Si was measured in the olivine core's soil exchangeable fraction, which compares to 132 µg/g Mg. Importantly, whereas the olivine-treated column's exchangeable fraction contains excess Mg compared to the control, this was not the case for Si (Supplementary Table 5). This means that the additional Si released from the olivine was likely not retained through adsorption.

Less Mg leaves the olivine-treated than the control core after 23 days of experimental time (Figure 3A). As mentioned above, as the likely dissolution of the Mg-rich forsterite should supply the core with additional Mg, an opposite behaviour would be expected shortly after 3.3 days (which is the residence time of waters in the columns). Hence, there appears to be a mechanism that keeps magnesium within the olivine-treated column in such amounts that even more than the additional Mg released from the dissolving olivine is retained. In consequence, olivine-derived Mg does not reach the effluent solution. As the only difference between the cores is the addition of olivine, it

can be concluded that the retention mechanism, which exerts higher control in the olivine-amended column, is increased by changes in soil chemistry induced by the dissolving forsterite. These changes might for example be related to the increase in pH (Figure 2), which facilitates cation exchange or, although subordinate, to the formation of secondary clays due to incongruent weathering of the olivine, which would provide additional surface sites (Gillman, 1980). Accordingly, in the column treated with olivine, there were significantly higher amounts of Mg bound in exchangeable form compared to control (Supplementary Figure 1). We also note that the 23 days of experimental time is similar to the observed 19 days (or theoretically calculated 14 days) it took for the 19°C experiments to become distinct, which was also attributed to cation exchange with the exchangeable complex (Pogge von Strandmann et al., 2021). The additional Mg released from the dissolving olivine is hence clearly retained through sorption processes, but it is unclear if sorption is the only process at play, or how long the signal would eventually be retarded if the experiment would have been run longer. This will be further discussed below.

Figure 3C shows that the olivine core's [Si] is higher than control after day 28 and on average the difference between the cores increases. This moment coincides with when the pH values of the olivine core become higher than the control. This demonstrates that (i) the added olivine dissolves and (ii) the retention mechanism that affects Mg exerts a smaller influence over Si. The differing behaviour of Mg and Si is further illustrated by the Si/Mg ratio of the olivine-treated column's effluent waters, which increases during the experiment from 1.27 to 5.51. The dissolution of forsterite should display a stoichiometric Si/Mg ratio (Wimpenny et al., 2010; as observed at 19°C) of ~1:2. The most likely mechanism that affects Mg, rather than Si, is again the adsorption to negatively charged surface sites. Hence, the addition of olivine and concomitant changes in soil chemistry lead to enhanced retention of Mg known to be affected by the soil cation exchange complex (e.g., Tipper et al., 2021).

### Exchangeable fraction leach at 19°C and 32°C further emphasises the importance of cation exchange in the context of EW

The importance of the exchangeable complex at high temperatures becomes further apparent when comparing the results of the sequential leaches at 19°C and 32°C. At higher temperatures, significantly more Mg was displaced by sodium acetate in the olivine-treated columns than at lower temperatures, as indicated by higher  $\Delta M_{\text{olivine-control}}$  values at 32°C than at 19°C (Figure 7A). This might be a combined effect of both faster olivine dissolution at higher temperatures, as well as an increased cation exchange capacity. Moreover, since no olivine was added to the control columns, they are assumed to be equal; however, at higher temperatures, higher amounts of Mg are adsorbed to exchange sites as well (Figure 7B). In this context, one should also consider the results of the mass balance calculations (Figure 6), which indicate a minimal influence of dissolving soil silicates and an attenuated carbonate control on the effluent solution. Even though surface equilibria between bulk solution and negatively charged surface sites are achieved quickly in a timescale of hours (Wada and Harada, 1971; Cai et al., 2022), slow diffusion, e.g., to the interlayers of clay

minerals can be a limiting factor (Blume et al., 2016). Here, faster kinetics at higher temperatures might lead to the observed increase of the exchangeable fraction due to faster diffusion of ions to interlayer exchange sites. Furthermore, clay minerals might be subject to structural alteration. For instance, Si-OH bonds might be broken up which leads to a population increase of free surficial functional groups, which would in turn increase the negative surface charge (Wada and Harada, 1971) and allow for more cation adsorption. Also, as more olivine dissolves at higher temperatures, the concomitant soil chemistry changes such as an increase in pH are more pronounced and could further increase cation exchange. An increase in cation exchange capacity was, for example, also observed in highly weathered soils when amended with basalt (Anda et al., 2015) and in soil column experiments using olivine (te Pas et al., 2023). The observed important effect of cation exchange is hence either controlled through temperature “directly” enhancing cation exchange or “indirectly” via rapid olivine dissolution and the soil changes it causes. In any case, our results show that cation exchange plays an important role in the context of enhanced weathering, especially in high temperature regimes, and potentially limits the applicability of cations as a quantification tool of sequestration rates through retention and thus signal retardation. This should be considered when interpreting data from field experiments. However, an increased cation exchange capacity and concomitant enhanced retention of nutrients could improve soil quality and prove beneficial for plant growth, in addition to the direct fertilising effect by silicate-derived nutrients. A comparison

of the exchangeable fraction between post-treatment and pre-treatment cores is shown in Supplementary Figure 1.

## Secondary clay formation

The formation of secondary clays could represent a further sink of Mg (and possibly also Si) as they are oversaturated in the effluent solutions. Their saturation indices increase in the olivine-treated column due to the rising pH and additional cation input from the dissolving olivine (Figure 4). Previous experiments however showed that clay mineral formation does not play a significant role on the short timescales of our experiments, especially when using through-flow experiments containing soils with pre-formed clays. At 19°C, therefore, the effects of uptake by clay were largely masked by processes related to the exchange complex and carbonate dissolution (Pogge von Strandmann et al., 2021). In other soil column experiments, clay formation was likewise not observed (te Pas et al., 2023). Nevertheless, clays (or at least their amorphous precursors) are almost certainly forming. Experiments starting with unweathered basalt (Pogge von Strandmann et al., 2019, 2022) show clay formation within a few hours, and the CarbFix experiment shows clay formation within a few days (Oelkers et al., 2019). Still, further analyses of, e.g., Mg isotopes, which fractionate during secondary clay formation, is needed to conclusively infer whether this took place in this particular high temperature experiment, but the formation of significant amounts of clay is not to be expected.

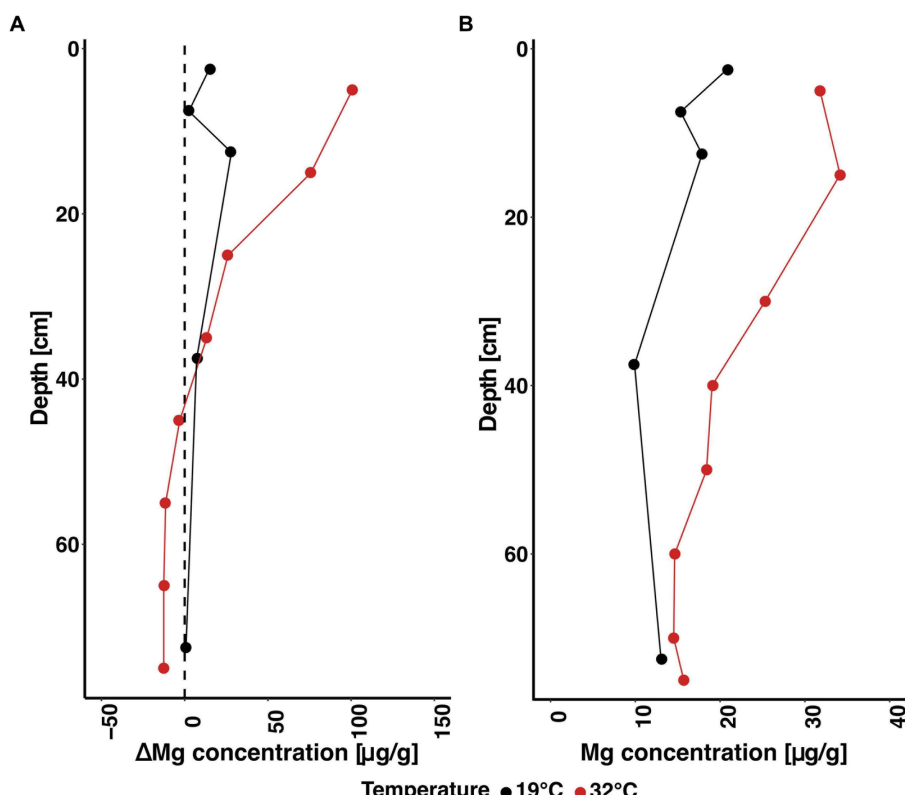


**FIGURE 7**  
Elemental concentrations of the exchangeable fraction at 19°C (Renforth et al., 2015) and this experiment (32°C) extracted through sequential leaching (Tessier et al., 1979). The left plot (A) shows  $\Delta\text{Mg}_{\text{ol-ctt}}$ . The right plot (B) displays Mg concentrations of the control columns at both temperatures.

## Retention behaviours of Mg and Si vary depending on temperature

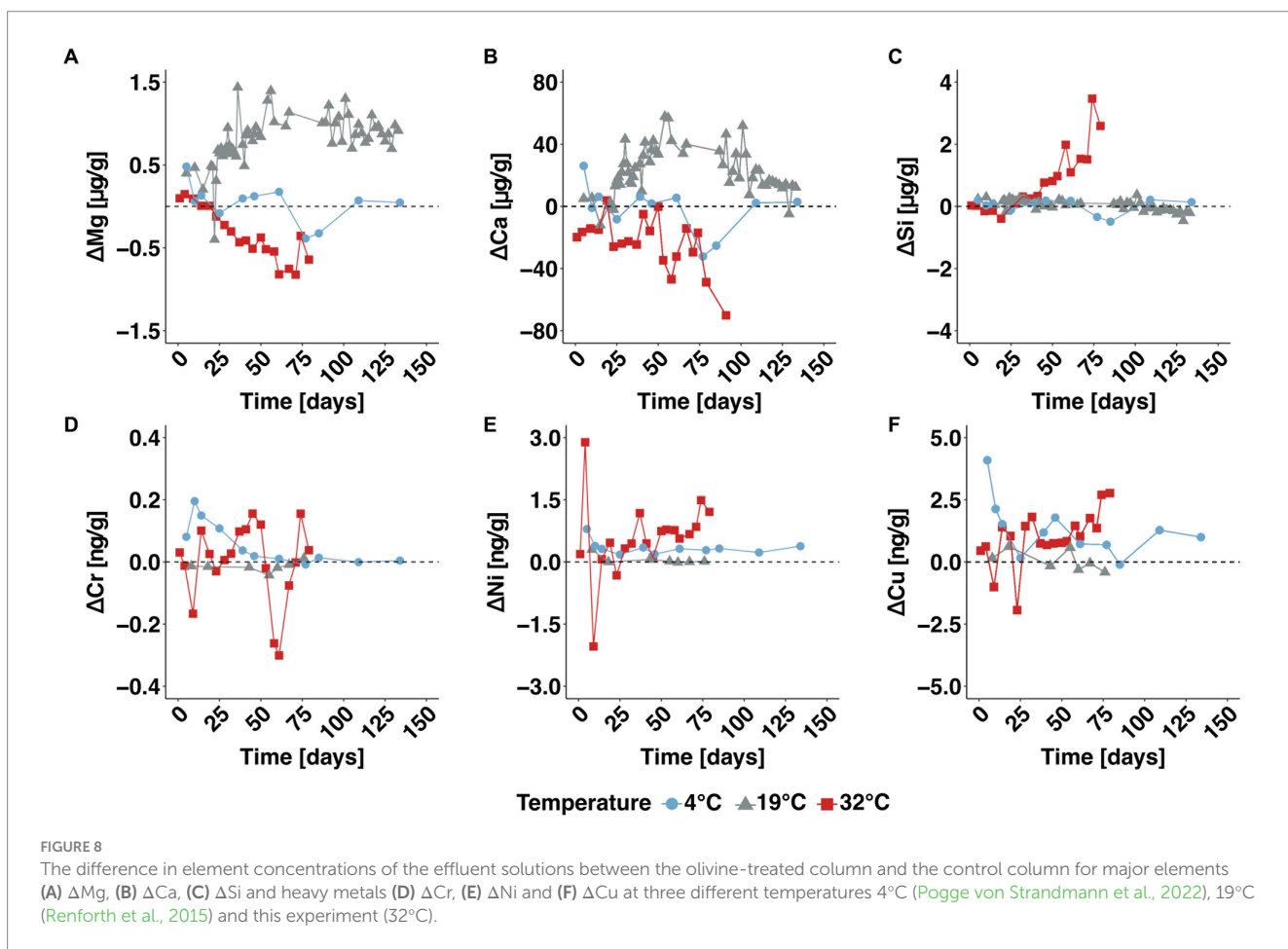
Figure 8 depicts  $\Delta X_{\text{olivine-control}}$  at 4°C, 19°C and 32°C (where X stands for the element measured from the effluent solution). Mg (Figure 8A), exhibits contrasting behaviours at different temperatures. The average propagated analytical uncertainty on  $\Delta X_{\text{olivine-control}}$  is 5.3% in the 32°C experiment, 7.5% at 19°C and 2.3% at 4°C. At 32°C, the olivine-derived Mg is likely completely retained within the core through secondary processes. Retardation was also observed in the 19°C experiment, where the olivine-treated column's effluent Mg concentration became resolvably higher than control only after 17 days, i.e., olivine-derived Mg eventually reached the effluent solution (Pogge von Strandmann et al., 2021). In our high temperature experiment, retardation is considerably longer at >70 days and olivine-derived Mg did not observably leave the core. Initially, the 4°C and 19°C experiments are similar which can be attributed to the availability of fresh outer surfaces of the added olivine powder (Anbeek, 1992).

Interestingly, Ca exhibits a relatively similar pattern to Mg (Figure 8B), although almost no additional Ca was added through the amendment with olivine, which suggests that Mg and Ca respond similarly towards the different retention mechanisms. This agrees with their similar mobility observed during natural weathering (e.g., Gislason et al., 1996).

Silicon shows an opposite trend compared to Mg (Figure 8C). Si preferentially leaves the core at 32°C and  $\Delta Si_{\text{olivine-control}}$  becomes positive, while  $\Delta Si_{\text{olivine-control}}$  at 19°C remains close to 0. Again at 4°C,

the very low  $\Delta Si_{\text{olivine-control}}$  values are due to the very limited dissolution of olivine at low temperatures, and thus no additional input of Si. The behaviour at 19°C, however, suggests a Si retention mechanism at moderate temperature conditions. This Si-consuming process could involve the formation of secondary amorphous Si-rich layers (Daval et al., 2011, 2013; Hellmann et al., 2012; Maher et al., 2016). Reprecipitation of these cation-depleted layers was, e.g., observed in an EW mesocosm experiment (Amann et al., 2020). Contrary to the 19°C experiment, the formation of such layers appears to be limited at 32°C, as  $\Delta Si_{\text{olivine-control}}$  shows an increasing trend, and this agrees with the observation of significant amounts of such amorphous silica forming during subglacial weathering (e.g., Hatton et al., 2019). At lower fluxes than in this experiment, the solutions will however likely be closer to equilibrium with the added mineral, and/or a passivating layer of secondary (clay) minerals that could form on the amendment mineral surface.

In summary, Mg is retained within soil cores at high temperatures and is eluted from soil cores at moderate temperatures, while the opposite behaviour is observed for Si, which preferentially leaves the core at high temperatures, but is retained at moderate temperatures. An amendment with silicates hence leads to changes in soil behaviour that also influence other mineral reactions. This implies that the behaviour of individual elements in the soil water solution should not be used universally to infer weathering rates of, in this case, olivine, as the strength of different retention mechanisms, which influence different elements to varying degrees, appears to change with temperature. When using silicate rock composed of different minerals,



the usability of a chemical cation weathering rate (CCWR) and especially a chemical silicate rock weathering rate (CSRWR; Hartmann and Moosdorf, 2011), incorporating major cations and silicon concentrations, would also be limited. The contrasting behaviour should be considered when interpreting field data from different temperature regimes.

## Trace element behaviour at low, moderate and high temperatures

Positive  $\Delta Ni_{olivine-control}$ ,  $\Delta Cr_{olivine-control}$  and  $\Delta Cu_{olivine-control}$  values at 32°C can again be interpreted as the release of weathering products following the dissolution of olivine (Figures 8D–F). The propagated analytical error is 7.53% for  $\Delta Ni_{olivine-control}$ , 6.14% for  $\Delta Cr_{olivine-control}$  and 2.26% for  $\Delta Cu_{olivine-control}$ . Strong fluctuations can be observed in the beginning, while later on, higher amounts of Ni and Cu leave the olivine-treated column. The reason for strong fluctuations and the strong negative excursion of Cr in the middle part of the 32°C experiment is unclear. It might be related to the system rapidly entering disequilibrium conditions due to the amendment of olivine. In general, the accumulation of metals in soils will be faster in tropical climates as a result of faster weathering at higher temperatures. As observed at 19°C, the retention of heavy metals appears to be high, and notably higher than in the 4°C experiment. Despite the effluent  $\Delta Ni_{olivine-control}$ ,  $\Delta Cr_{olivine-control}$  and  $\Delta Cu_{olivine-control}$  values being higher than at 4°C, the amount of heavy metals exiting the columns is less than anticipated, considering the accelerated weathering at elevated temperatures. Similarly, Raveh-Rubin et al. (2015) show evidence of fast Ni retention at higher temperatures with Ni becoming immobile for an extended period of time and laterites were shown to exhibit high Ni contents with serpentinite zones having up to >2% nickel (Lewis et al., 2006). This could be partly related to the increased availability of secondary clay minerals in the higher temperature columns, as well as to the mechanisms as discussed above for Mg. Furthermore, adsorption of heavy metals was found to be higher in the presence of Cr, released in our experiment from dissolving olivine, compared to the adsorption of the sole individual non-competing metal (Campillo-Cora et al., 2020). Heavy metals, including their toxicity, will be further discussed below.

## Olivine dissolution rates

### Mg-derived and Si-derived weathering rates

The olivine dissolution rate ( $W_r$ ) was calculated using a surface area normalised approach (Equation 2). It is important to note that for reasons described above, the values (being net values) are to some degree surrounded by uncertainty as the influence of the respective element-retaining mechanism is ambiguous. It is assumed that olivine amendment is the only variable that causes a difference between the olivine-treated column and control column (Renforth et al., 2015; Pogge von Strandmann et al., 2021, 2022). Although in the original studies at 4°C and 19°C, Mg concentrations of the column's effluent solutions could be used to quantify olivine dissolution, Mg is retained

within the olivine-treated column in this experiment. It is hence not possible to determine the weathering rate based on Mg, as  $\Delta Mg_{olivine-control}$  becomes negative. We therefore utilise Si, which appears to be less affected by retention. We furthermore apply this equation to the 19°C data (Renforth et al., 2015) and 4°C data (Pogge von Strandmann et al., 2022) to compare the Si-derived rates to those based on Mg (Figure 9). The equation thus reads:

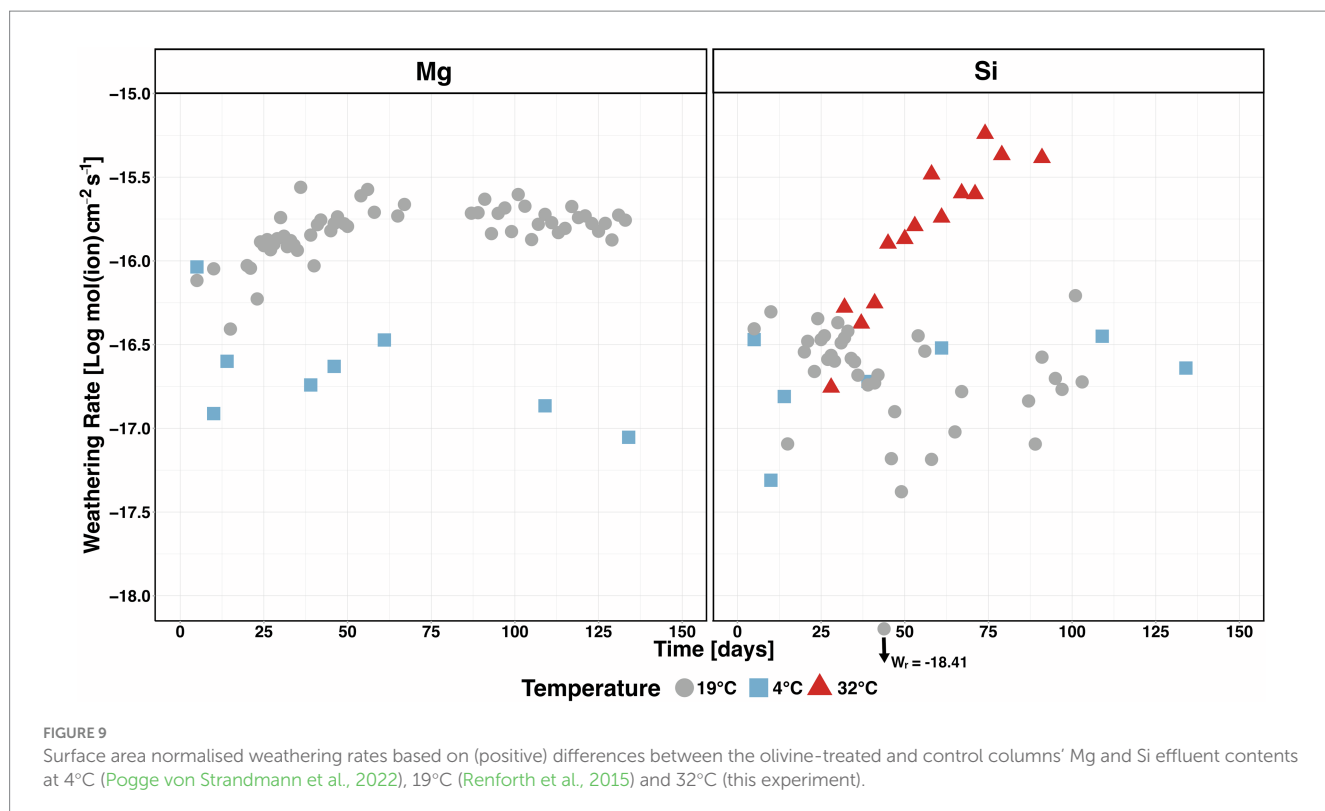
$$W_r = \frac{Q_{solution} \times \Delta Si_{olivine-control}}{SSA \times m_{olivine}} \quad (2)$$

where  $W_r$  denotes the surface area normalised dissolution rate ( $\text{mol(Si) cm}^{-2} \text{s}^{-1}$ ),  $Q_{solution}$  the solution flux in  $\text{g s}^{-1}$ ,  $\Delta Si_{olivine-control}$  the difference between molar concentrations of Si in the effluent solutions of the olivine-treated and control core in  $\text{mol g}^{-1}$ , SSA the BET surface area of the olivine ( $\text{cm}^2 \text{g}^{-1}$ ,  $3.04 \times 10^4$ ) as determined by Renforth et al. (2015) and  $m_{olivine}$  the mass of the added olivine [g].

At 4°C, incipient weathering and a subsequent rapid reduction of  $W_r$  can be conclusively inferred using the Mg-derived rate (Figure 9). Contrastingly, such initially fast weathering at 4°C is not seen in the Si-based values, which are in a similar range throughout the experiment ( $10^{-16.47} \text{ mol(Si) cm}^{-2} \text{s}^{-1}$  at the beginning and  $10^{-16.64} \text{ mol(Si) cm}^{-2} \text{s}^{-1}$  at the end). The Mg-derived weathering rate of the 19°C experiment starts at  $10^{-16.10} \text{ mol(Mg) cm}^{-2} \text{s}^{-1}$  and then increases slightly, before stabilising at  $10^{-15.80} \text{ mol(Mg) cm}^{-2} \text{s}^{-1}$  after  $\sim 50$  days. The Si-based 19°C  $W_r$  is significantly lower than the Mg-derived  $W_r$  (max.  $10^{-16.21} \text{ mol(Si) cm}^{-2} \text{s}^{-1}$  and min.  $10^{-18.41} \text{ mol(Si) cm}^{-2} \text{s}^{-1}$ ), which is similar to 4°C, where weathering was found to be highly limited due to the low temperatures (Figure 9). This is most likely related to the above-described retention of Si which we observe at 19°C and emphasises that in our experiments, Si fluxes cannot be used to calculate  $W_r$  at moderate temperatures. In contrast, the Si-based  $W_r$  at 32°C shows a clear increasing trend after  $\Delta Si_{olivine-control}$  becomes positive from day 28 onwards ( $10^{-16.76} \text{ mol(Si) cm}^{-2} \text{s}^{-1}$  at the start and  $10^{-15.38} \text{ mol(Si) cm}^{-2} \text{s}^{-1}$  at the end of the experiment). It is unclear whether a longer experimental duration would lead to a continuous increase or whether the rate would level off at a certain point as observed at 19°C when using Mg to infer  $W_r$ . Hence, the weathering rate determined in this experiment should be considered a conservative estimate, with the true values possibly higher.

### The temperature dependence of olivine dissolution rates under natural and laboratory conditions

Figure 10 shows the average surface area normalised weathering rates ( $W_r$ ) at 4°C, 19°C and 32°C based on Mg and Si as closed circles, vertical box dimensions show the interquartile range, whiskers the propagated analytical error on the daily element flux (Equation 3), while the horizontal line within the boxes indicates the median. The average  $W_r$  at 4°C is  $10^{-16.70} \text{ mol(Si) cm}^{-2} \text{s}^{-1}$ , at 19°C  $W_r=10^{-16.71} \text{ mol(Si) cm}^{-2} \text{s}^{-1}$  and at 32°C  $W_r=10^{-15.83} \text{ mol(Si) cm}^{-2} \text{s}^{-1}$ . The anticipated weathering rate, based on the Mg-derived dissolution rates of the lower temperature experiments represented by the open square is considerably higher compared to its Si-based counterpart (average  $W_r=10^{-15.09} \text{ mol(Mg) cm}^{-2} \text{s}^{-1}$ ). For this, we assume similar behaviour as in Oelkers et al. (2018).



The propagated analytical uncertainty ( $\sigma_p^2$ ) on the daily effluent element flux ( $\mu\text{g/day}$ ) is calculated according to Equation 3:

$$\sigma_p^2 = (t_2 - t_1)^2 \sigma_1^2 / 4 + (t_n - t_{n-1})^2 \sigma_n^2 / 4 + \sum_{i=2}^{n-1} (t_{i+1} - t_{i-1})^2 \sigma_i^2 / 4, \quad (3)$$

where  $t$  is the time at the  $i$ th data point and  $A$  analytical uncertainty.

Furthermore, a theoretical T-dependent dissolution rate, based on disequilibrium laboratory experiments (Oelkers et al., 2018),  $W_{r\_lab}$  is calculated using Equation 4 and indicated by the black line.

$$W_{r\_lab} = A a_{H^+}^n e^{-E_a / RT} \quad (4)$$

Here,  $R$  is the gas constant ( $8.3145 \text{ kJ mol}^{-1} \text{ K}^{-1}$ ),  $E_a$  is the activation energy ( $52.9 \pm 6.9 \text{ kJ mol}^{-1} \text{ K}^{-1}$ ),  $A$  is a pre-exponential factor of 0.0854,  $n$  the reaction with respect to  $\text{H}^+$  = 0.46,  $T$  the temperature in K and  $a$  the activity (Pokrovsky and Schott, 2000; Hänen et al., 2006).

First, as expected, the weathering rate increases with temperature. Second, Mg-derived dissolution rates are higher than Si-derived values. However, at 4°C, the difference is only marginal, as at low temperatures, weathering was found to be very limited and differences are hence not as high compared to higher temperatures and concomitant higher weathering rates. The disparity between (expected) Mg-derived and Si-derived  $W_r$  is highest at elevated temperatures (Figure 10), marking a distinct difference between the (expected) Mg-derived dissolution rate and the observed Si-derived at 32°C.

As anticipated, weathering rates derived in this experiment are an order of magnitude lower than idealised rates. This can most likely

be attributed to (i) a higher fluid/mineral ratio in conventional laboratory studies enabling effective solute transport from the mineral surface and (ii) far-from-equilibrium conditions in laboratory experiments. Contrastingly, in this experiment, the contact between mineral and fluid might be limited in the soil and conditions are much closer to equilibrium than in laboratory experiments. The difference between both Mg-derived and Si-derived rates and laboratory-derived rates clearly emphasises that laboratory-derived rates should not be used to quantify olivine dissolution in EW-measures. While it generally is easier to carry out measurements of (single) cations in field settings compared to, e.g., analysing anticipated small changes in alkalinity, the difference between Si-derived and Mg-derived  $W_r$  hence further indicates that cations alone should ideally not be used for quantification of EW measures in field conditions.

## Enhanced weathering as a negative emission technology

### Shrinking core model

Some of the biggest uncertainties surrounding enhanced weathering approaches are the energy requirements for material comminution needed to achieve sufficient weatherable surface areas for the desired  $\text{CO}_2$  sequestration rates. Hence, it is important to estimate the extent of dissolution ( $X$ ) as function of time ( $t$ ) for particles of different initial diameters ( $D_0$ ; m) for different dissolution rates ( $W_r$ ;  $\text{mol}(\text{olivine}) \text{ m}^{-2} \text{ s}^{-1}$ ) using a shrinking core model (Equation 5).  $V_m$  is the molar volume of the material ( $\text{m}^3 \text{ mol}^{-1}$ ) and  $t$  the dissolution time (s; Hangx and Spiers, 2009; Renforth et al., 2015; Pogge von Strandmann et al., 2022). From this, dissolution timescales of particles with differing average

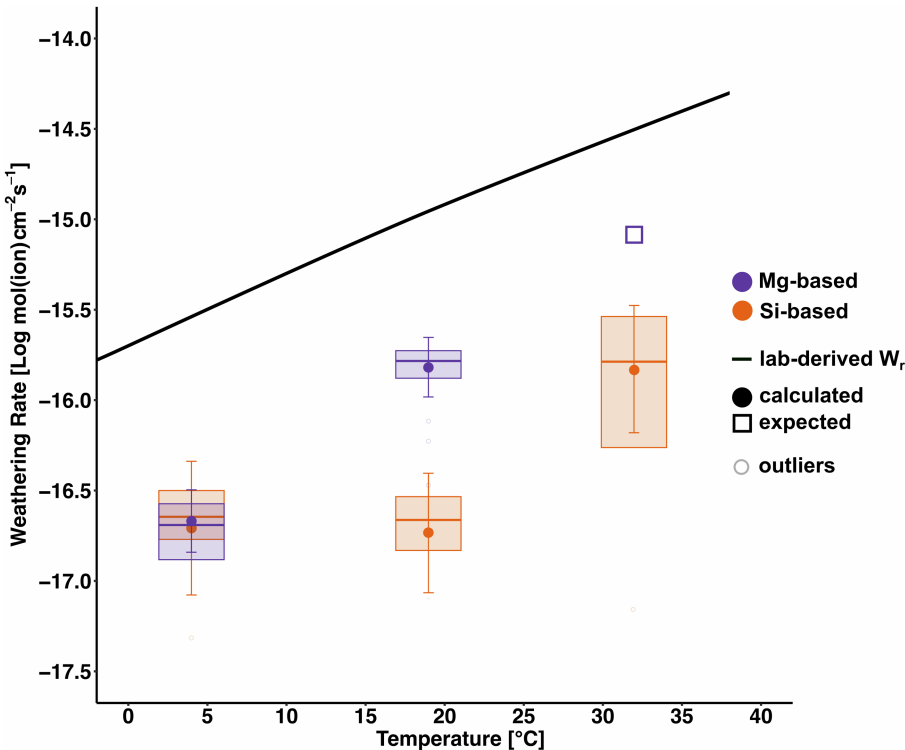


FIGURE 10

Box-whisker plots of weathering rates at 4°C (Pogge von Strandmann et al., 2022), 19°C (Renforth et al., 2015) and 32°C (this experiment). Mean  $W_r$  values are shown as closed circles, vertical box dimensions show the interquartile range, whiskers the propagated analytical error on the daily element flux (Equation 4), while the horizontal line within the boxes indicates the median. Outliers are defined as any values over 1.5 times below the first quartile or above the third quartile. The idealised temperature-dependent dissolution of forsterite is shown as a black line. As it was not possible to calculate the Mg-based weathering rate at 32°C due to the retention of Mg in the core, an expected value based on the dissolution behaviour of olivine in Oelkers et al. (2018) is displayed as an open square.

diameters can be derived. The results for six different average weathering rates at 4°C, 19°C and 32°C as shown in Figure 10, based on Mg and Si, respectively, are depicted in Figure 11 (note that the Mg-derived rate at 32°C is based on a calculated rate, rather than a measured one).

$$X(t) = \frac{D_0^3 - (D_0 - 2W_r V_m t)^3}{D_0^3} \quad (5)$$

As grinding does not result in a single particle size, the equation is integrated over a normalised gamma particle size distribution (Equation 6), as previously used in shrinking core models (Gbor and Jia, 2004; Renforth et al., 2015; Pogge von Strandmann et al., 2022). Here,  $\alpha$  and  $\beta$  are empirically derived coefficients which describe the variability of particle size.

$$\Gamma(D) = \frac{D^{\alpha-1} e^{-D/\beta}}{\beta^\alpha \Gamma(\alpha)} \quad (6)$$

The weathering rates obtained here are likely lower than in reality, due to the nature of the calculation based on weathering-derived cations rather than direct measurements of alkalinity. Further, as

mentioned above, this experiment does not take into account biochemical processes and reactions that occur in a real field setup, which may have profound effect on dissolution speed. Nonetheless, given that a standardised method for quantifying weathering rate in the context of EW has yet to be developed, these findings offer an approximate understanding of the time frames within which the weathering reactions occur. Lower rates have been found in a mesocosm experiment that aimed to simulate further naturally occurring processes (Amann et al., 2020).

Based on Si a grain size of 125 µm at 32°C takes ~4,000 years for 80% of particles to dissolve and ~1.7 years until 20% are dissolved. On the other hand, for smaller-sized particles averaging around 10 µm (the grain size used by the modelling study of Taylor et al., 2016), it takes ~32 years for 80% dissolution and less than a year until 20% are dissolved. 80% of 1 µm particles dissolve in ~10 years and 20% in ~0.7 years.

Dissolution times expected for Mg are notably shorter when compared to those based on Si. For a particle size of 125 µm, 80% dissolve after 740 years, while 20% are dissolved after 0.3 years. For 10 µm, 20% dissolution is achieved after only ~0.2 years, while 80% are dissolved after around 6 years. 80% of 1 µm particles dissolve in ~1.8 years and 20% very quickly in ~0.2 years. These findings indicate that initial weathering is very rapid but it takes considerable time until full dissolution is achieved.

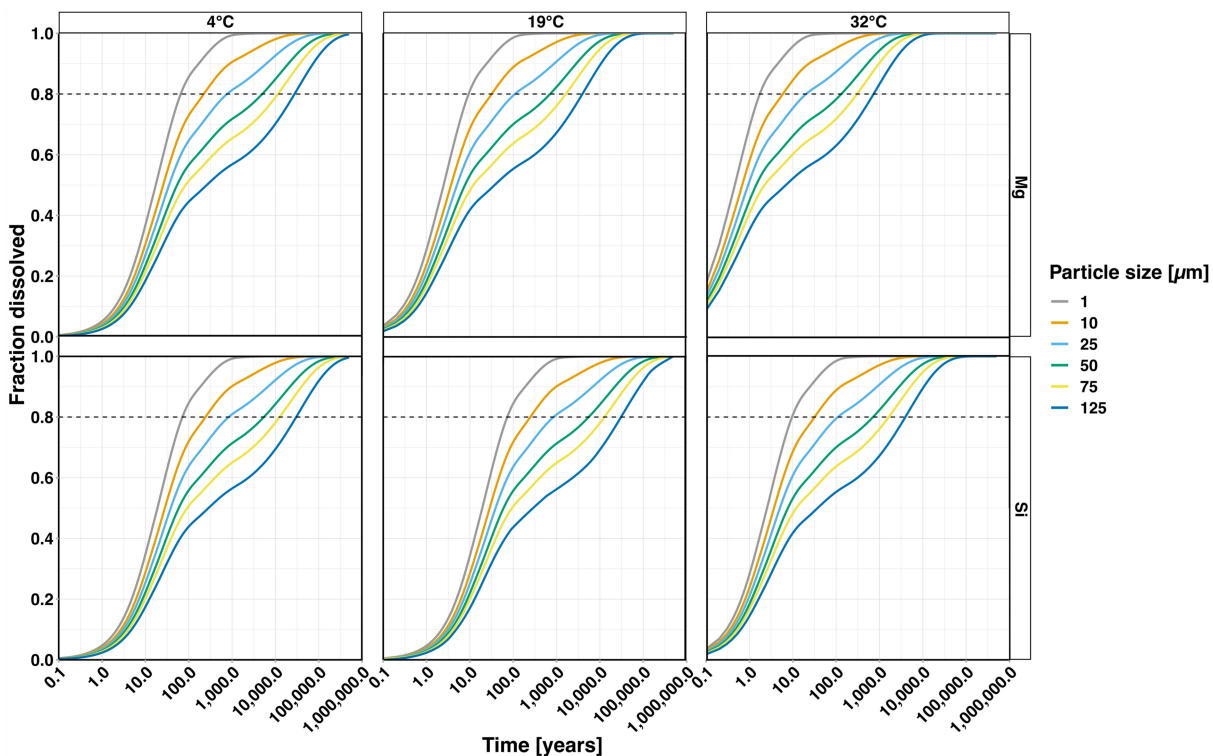


FIGURE 11

Modelled degree of dissolution for a range of olivine grain sizes based on a shrinking core model (see text for details). The horizontal dashed lines represent a dissolved fraction of 80% (as the last 20% require a considerable amount of time to eventually dissolve).

In general, dissolution times are higher at lower temperatures, and again, dissolution time estimations based on Mg shorter than those based on Si, due to dissolution rates increasing with temperature (Figure 10) and retention of Si at moderate temperatures due to secondary processes. Taylor et al. (2016) modelled an annual amendment of tropical soils with weatherable material having a uniform grain size of 10  $\mu\text{m}$ . Mg-derived weathering rates can be regarded the maximum values in our experiment. As our dissolution times at 32°C, which is higher than the mean annual temperature of tropical soils of  $\sim 22^\circ\text{C}$  (Lembrechts et al., 2022), exceed 1 year, annual amendments may thus possibly not be feasible as they would result in accumulation of unweathered material based on our data. Comminution to even smaller average grain sizes than 1  $\mu\text{m}$  might be needed, which would currently result in additional emissions from electricity supply (Renforth, 2012), but likely reduced as the power grid decarbonises.

## CO<sub>2</sub> sequestration potential

The primary aim of this experiment is to explore the fate of cations within the soil, which control CO<sub>2</sub> removal and charge-balance alkalinity. In principle, they are also easier to measure in the field compared to the anticipated small changes in alkalinity. However, inferring CO<sub>2</sub> sequestration indirectly from weathering-derived cations requires several assumptions, and as we show here, can also be strongly affected by the soil's cation exchange capacity. Nonetheless, in the following we calculate the sequestration potential of olivine added to agricultural lands based on the weathering rates derived in

this experiment. Pogge von Strandmann et al. (2022) calculated the possible maximum carbon dioxide capture potential of the olivine used in this experiment (EW<sub>p</sub>) utilising the modified Steinour equation and olivine elemental concentrations assessed via XRF at EW<sub>p</sub> = 0.79 tCO<sub>2</sub>/t. Using Equation 3 from Renforth et al. (2015), which converts net olivine dissolution rates into expected spatial area normalised dissolution rates, and applying EW<sub>p</sub>, the average Si-based W<sub>r</sub> at 4°C of  $10^{-16.70}$  mol(Si) cm<sup>-2</sup> s<sup>-1</sup>,  $10^{-16.71}$  mol(Si) cm<sup>-2</sup> s<sup>-1</sup> at 19°C and  $10^{-15.83}$  mol(Si) cm<sup>-2</sup> s<sup>-1</sup> at 32°C equate to carbon dioxide capture potentials of  $\sim 15$  t CO<sub>2</sub> km<sup>-2</sup> year<sup>-1</sup> at 4°C and 19°C, and  $\sim 115$  t CO<sub>2</sub> km<sup>-2</sup> year<sup>-1</sup> at 32°C, respectively. The max. observed W<sub>r</sub> of  $10^{-15.24}$  mol(Si) cm<sup>-2</sup> s<sup>-1</sup> in this experiment corresponds to  $\sim 450$  t CO<sub>2</sub> km<sup>-2</sup> year<sup>-1</sup>. These calculations assume an amendment rate of 12.7 kg m<sup>-2</sup>. Note that these calculations do not take into account changes in olivine surface area and that the experimental periods of the lower temperature experiments were longer. Further, the alkalinity-enhancement carbon drawdown pathway (Buckingham et al., 2022; West et al., 2023) and the biotic pathway of EW (Goll et al., 2021) are not covered in this experiment as biota (plants, fungi, microbes and macro-vertebrates such as earth worms) can strongly affect weathering rates and physicochemical soil processes (Versteegh et al., 2014; Verbruggen et al., 2021; Vicca et al., 2022; Vienne et al., 2023). As mentioned above, the sequestration potential inferred in this study should hence be regarded a conservative estimate, which might also be indicated by ambient condition carbon dioxide sequestration rates of dunite and ultramafic lithologies, respectively, being higher than the high temperature consumption rates obtained in this experiment (Schopka et al., 2011; Amann et al., 2022).

## Heavy metal toxicity

In the context of enhanced weathering, the release of potentially toxic metals is possible and represents one of the most important potential limiting factors of this method. Several authors have pointed out that the build-up of such elements might pose inadvertent environmental risks (Renforth, 2012; Hartmann et al., 2013; Renforth et al., 2015; Haque et al., 2020; Flipkens et al., 2021; Pogge von Strandmann et al., 2022). Such risks might limit the feasibility of enhanced weathering (EW) as a negative emissions technology. Assessing these risks, especially at high temperatures that lead to rapid weathering, is therefore of great importance. We use the European Union's human drinking water standard (98/83/EC) and thresholds set in the Finnish legislation. These Finnish threshold values serve as a reliable estimate of the average values found in different European national systems (Carlon, 2007) and have been adopted on an international scale for agricultural soils (Voet et al., 2013). As above, we assume an amendment of  $12.7 \text{ kg/m}^2$  olivine as in Renforth et al. (2015) and Pogge von Strandmann et al. (2022) and constant dissolution rates for retention efficiency, soil accumulation and drinking water contamination calculations.

The European Union's human drinking water standard is  $50 \text{ ng/mL}$  Cr. The maximum value of the solution leaving the olivine-treated column would be  $1.73 \text{ ng/mL}$  and hence, ~30 times lower than threshold. Using a Si/Cr ratio of 2035, measured on our amendment olivine (Renforth et al., 2015), it can be assessed that over the course of the experiment,  $\sim 55 \mu\text{g}$  Cr were released from the added olivine, while the difference between the olivine-treated column and control column is  $\sim 0.34 \mu\text{g}$ . Hence, >99% of the released Cr was retained within the core. This is clearly higher than the retention efficiency of ~26% at  $19^\circ\text{C}$  and ~34% at  $4^\circ\text{C}$ . The Finnish Ministry of Environment gives a limit of  $200 \text{ mg/kg}$  Cr for soils. Taking into account a background concentration of  $50 \text{ mg/kg}$  (Ertani et al., 2017) and assuming complete retention of the released Cr, it would take ~6,800 years to reach this threshold. Background concentrations of Cr in agricultural soils are however highly variable and have been observed to reach above-limit values of up to  $350 \text{ mg/kg}$  (Ertani et al., 2017). Given our earlier experiments' retention of Cr, it would take over 1.5 million years at  $4^\circ\text{C}$  and ~33,000 years at  $19^\circ\text{C}$  of this level of enhanced weathering to breach these limits.

Similarly, a Si/Ni ratio of ~72 can be used to infer a total  $\sim 1,573 \mu\text{g}$  Ni released from the olivine during the experimental period, which compares to a  $\sim 14 \mu\text{g}$  difference between both cores and likewise gives a retention efficiency of >99%, similar to those at  $19^\circ\text{C}$  and  $4^\circ\text{C}$ , which are ~99% and ~90%, respectively. European drinking water standards in case of Ni are  $20 \text{ ng/mL}$ . The maximum value in the effluent waters is  $\sim 11 \text{ ng/mL}$  and hence lower than the guideline. In mesocosm (Amann et al., 2020) and soil column (te Pas et al., 2023) enhanced weathering experiments, Ni was found to exceed the limits of drinking water quality. In this experiment, the Ni concentration in the effluent solution reaches a level where the threshold could potentially be met or exceeded, for example when the soil is amended with greater amounts of olivine, olivine-rich rocks with higher Ni contents or when repeated annual amendment is carried out. Regarding accumulation in the soil, the Finnish guideline is  $100 \text{ mg/kg}$  Ni. Assuming an average European background concentration of Ni of  $37 \text{ mg/kg}$  (Agyeman et al., 2022), it would take ~100 years to exceed the threshold if all Ni

associated with the olivine dissolution were retained. Realistically, however, parts of the released heavy metals would be exported from the amendment area in dissolved form. At  $4^\circ\text{C}$ , it would take ~10,000 years to reach the threshold, and ~126 years at  $19^\circ\text{C}$ .

An olivine Si/Cu ratio of ~176 is used to calculate a total  $\sim 640 \mu\text{g}$  Cu that is released during the dissolution of the added olivine. 81% of Cu is retained within the core. The drinking water threshold of  $2000 \mu\text{g/L}$  is far from being exceeded at a maximum of  $18 \mu\text{g/L}$  in the effluent solution. Assuming an average Cu background concentration of  $17 \text{ mg/kg}$  in Europe (Ballabio et al., 2018), it would hence require ~522 years until the lower soil limit of  $150 \text{ mg/kg}$  was reached in the extreme case that all olivine-derived Cu was retained.

To sum up, although heavy metal accumulation is faster in the high temperature  $32^\circ\text{C}$  experiment than at  $19^\circ\text{C}$  and  $4^\circ\text{C}$ , the amendment of agricultural soils with olivine appears to be rather safe with the exception of Ni in drinking water, which exhibits alarmingly high values in the solution exiting the olivine-treated core.

## Conclusion and outlook

This study identifies the influence of complex temperature-dependent soil processes, which contrastingly affect Mg and Si. Measurements of single elements, although easier to carry out in field settings than direct measurements of alkalinity (where changes due to EW are also difficult or impossible to detect) and therefore theoretically of interest for commercial applications, should thus not be used to derive sequestration rates in the context of EW. At moderate temperatures, Mg preferentially leaves the core while Si is retained. The opposite is observed at high temperatures, where Si leaves the core and Mg is retained. This implies different retention mechanisms which affect Mg and Si to different extents and are dependent on temperature. Si-retention at moderate temperatures might be caused by the formation of secondary clays or Si-rich amorphous layers, while cation exchange is identified as at least one of the Mg-retention mechanisms in the high temperature experiment. The addition of olivine enhances the cation exchange capacity of olivine-amended soil, and this effect appears to increase with temperature. At  $32^\circ\text{C}$ , this retaining effect is strong enough to prevent Mg from the dissolving olivine from reaching the effluent waters throughout the 79-day experiment. This retention period is considerably longer than the breakthrough time at  $19^\circ\text{C}$  of 17 days and can be considered a minimum retention time. We thus show that cation exchange plays an important role on the timescales at which enhanced weathering operates. Cation exchange and concomitant signal retardation should therefore also be considered in the interpretation of enhanced weathering field trials, especially in high temperature regions, which would include the majority of global "weathering hotspots" best suited for enhanced weathering.

While the strong influence of exchange processes is remarkable, and high amounts of Mg are retained adsorbed to negatively charged surfaces, it is unclear to which extent further Mg was incorporated into secondary silicates, carbonates, and oxides or specifically adsorbed as inner-sphere complexes, which would render Mg non-exchangeable. Here, the utilisation of stable "non-traditional" isotope measurements might provide further insights into the fate of weathering-derived cations.

As anticipated, the dissolution rate of olivine increases with increasing temperature and ideal laboratory inferred dissolution rates

are significantly higher than those observed here in soils. This can be attributed to near-equilibrium conditions, lower material/solution ratios, mineral encapsulation, cation retention due to adsorption, higher pH or stabilisation of soil organic matter in this experiment. As seen in other studies, simple laboratory weathering rates are not suited to quantify enhanced weathering rates in natural conditions, however, could be used to understand important reactions through soil and into drainage waters. Furthermore, surface area normalised Si-derived dissolution rates are lower than those based on Mg, and both should be regarded as conservative estimates.

A shrinking core model indicates that even at highly elevated temperatures (32°C), the dissolution time of olivine in soils with an average grain size of 1 µm exceeds 1 year, and the comminution to sufficiently small grain sizes <1 µm would entail considerable energy requirements. The dissolution of 10 µm particles in <10 years suggests that enhanced weathering has clear potential as a negative emissions strategy, but is unlikely to be able to be used with the frequency that some model calculations imply.

Accumulating heavy metals do not exceed Finnish soil (acting as an approximate value of European national guidelines) and EU drinking water thresholds. However, Ni concentrations in the effluent solution are elevated and if an olivine with higher Ni contents were used, drinking water guidelines might be exceeded and could potentially pose a risk to human health in (sub-)tropical regions in which enhanced weathering will effectively be carried out. Dangerously high accumulation of Cr, Ni or Cu in the soil is, however, unlikely.

## Data availability statement

The original contributions presented in the study are included in the article/[Supplementary material](#), further inquiries can be directed to the corresponding author.

## Author contributions

NI conducted the experiment, performed the analyses and calculations, interpreted the data and wrote the manuscript. PP

## References

- Agyeman, P. C., Kebonye, N. M., John, K., Borůvka, L., Vašát, R., and Fajemisim, O. (2022). Prediction of nickel concentration in peri-urban and urban soils using hybridized empirical bayesian kriging and support vector machine regression. *Sci. Rep.* 12, 3004–3016. doi: 10.1038/s41598-022-06843-y
- Amann, T., Hartmann, J., Hellmann, R., Pedrosa, E. T., and Malik, A. (2022). Enhanced weathering potentials—the role of in situ CO<sub>2</sub> and grain size distribution. *Front. Climate* 4. doi: 10.3389/fclim.2022.929268
- Amann, T., Hartmann, J., Struyf, E., De Oliveira Garcia, W., Fischer, E. K., Janssens, I., et al. (2020). Enhanced weathering and related element fluxes - a cropland mesocosm approach. *Biogeosciences* 17, 103–119. doi: 10.5194/BG-17-103-2020
- Anbeek, C. (1992). The dependence of dissolution rates on grain size for some fresh and weathered feldspars. *Geochim. Cosmochim. Acta* 56, 3957–3970. doi: 10.1016/0016-7037(92)90009-8
- Anda, M., Shamshuddin, J., and Fauziah, C. I. (2015). Improving chemical properties of a highly weathered soil using finely ground basalt rocks. *Catena (Amst)* 124, 147–161. doi: 10.1016/j.catena.2014.09.012
- Andrews, M. G., and Taylor, L. L. (2019). Combating climate change through enhanced weathering of agricultural soils. *Elements* 15, 253–258. doi: 10.2138/gselements.15.4.253
- Ballabio, C., Panagos, P., Lugato, E., Huang, J. H., Orgiazzi, A., Jones, A., et al. (2018). Copper distribution in European topsoils: an assessment based on designed the project, conducted the experiment and interpreted the data. PR designed the project and interpreted the data. All authors contributed to the article and approved the submitted version.
- We thank Carolin Berg and Regina Walter for assistance during the chemical analyses and Anne Jantschke, Benedikt Schneider and Ralf Meffert for performing the XRD analyses. JGU Mainz is thanked for the MSc of NI. PS acknowledges ERC grant 682760 CONTROLPASTCO<sub>2</sub>, Carl Zeiss + German Scholars Organisation programme GSO/CZS 36, and DFG grant INST 247/1095-1. PR acknowledges UKRI funding in the ‘Greenhouse gas removal with UK agriculture via enhanced rock weathering project’ (BB/V011359/1).
- The authors declare that the research was conducted in the absence of any commercial or financial relationships that could be construed as a potential conflict of interest.
- All claims expressed in this article are solely those of the authors and do not necessarily represent those of their affiliated organizations, or those of the publisher, the editors and the reviewers. Any product that may be evaluated in this article, or claim that may be made by its manufacturer, is not guaranteed or endorsed by the publisher.
- The Supplementary material for this article can be found online at: <https://www.frontiersin.org/articles/10.3389/fclim.2024.1252210/full#supplementary-material>
- LUCAS soil survey. *Sci. Total Environ.* 636, 282–298. doi: 10.1016/J.SCITOTENV.2018.04.268
- Béarat, H., McKelvy, M. J., Chizmeshya, A. V. G., Gormley, D., Nunez, R., Carpenter, R. W., et al. (2006). Carbon sequestration via aqueous olivine mineral carbonation: role of passivating layer formation. *Environ. Sci. Technol.* 40, 4802–4808. doi: 10.1021/ES0523340
- Berner, R. A. (2003). The long-term carbon cycle, fossil fuels and atmospheric composition. *Nature* 426, 323–326. doi: 10.1038/nature02131
- Blume, H.-P., Brümmer, G. W., Fleige, H., Horn, R., Kandeler, E., Kögel-Knabner, I., et al. (2016). Chemical properties and processes. *Scheffer/Schachtschabel Soil Sci.* 123–174. doi: 10.1007/978-3-642-30942-7\_5
- Brady, N. C., and Weil, R. R. (2016). *Nature and properties of soils*. 15th Edn. Columbus, Ohio: Pearson Education, 1104.
- Buckingham, F. L., Henderson, G. M., Holdship, P., and Renforth, P. (2022). Soil core study indicates limited CO<sub>2</sub> removal by enhanced weathering in dry croplands in the UK. *Appl. Geochem.* 147:105482. doi: 10.1016/j.apgeochem.2022.105482
- Cai, D., Henehan, M. J., Uhlig, D., and von Blanckenburg, F. (2022). Mg isotope composition of runoff is buffered by the regolith exchangeable pool. *Geochim. Cosmochim. Acta* 321, 99–114. doi: 10.1016/J.GCA.2022.01.011

## Acknowledgments

## Conflict of interest

## Publisher's note

## Supplementary material

- Calabrese, S., Wild, B., Bertagni, M. B., Bourg, I. C., White, C., Aburto, F., et al. (2022). Nano- to global-scale uncertainties in terrestrial enhanced weathering. *Environ. Sci. Technol.* 56, 15261–15272. doi: 10.1021/ACS.EST.2C03163
- Campillo-Cora, C., Conde-Cid, M., Arias-Estevez, M., Fernández-Calviño, D., and Alonso-Vega, F. (2020). Specific adsorption of heavy metals in soils: individual and competitive experiments. *Agronomy* 10:1113. doi: 10.3390/agronomy10081113
- Carlon, C. (2007). *Derivation methods of soil screening values in Europe. A review and evaluation of national procedures towards harmonization*. Ispra: European Commission, Joint Research Centre, Ispra, EUR 22805-EN, 306.
- Daval, D., Hellmann, R., Martinez, I., Gangloff, S., and Guyot, F. (2013). Lizardite serpentine dissolution kinetics as a function of pH and temperature, including effects of elevated pCO<sub>2</sub>. *Chem. Geol.* 351, 245–256. doi: 10.1016/j.chemgeo.2013.05.020
- Daval, D., Sissmann, O., Menguy, N., Saldi, G. D., Guyot, F., Martinez, I., et al. (2011). Influence of amorphous silica layer formation on the dissolution rate of olivine at 90°C and elevated pCO<sub>2</sub>. *Chem. Geol.* 284, 193–209. doi: 10.1016/j.chemgeo.2011.02.021
- Dessert, C., Dupré, B., Gaillardet, J., François, L. M., and Allègre, C. J. (2003). Basalt weathering laws and the impact of basalt weathering on the global carbon cycle. *Chem. Geol.* 202, 257–273. doi: 10.1016/j.chemgeo.2002.10.001
- Dietzel, M. (2002). “Interaction of polysilicic and monosilicic acid with mineral surfaces,” in *Water-Rock Interaction*. eds. I. Stober, and K. Bucher (Dordrecht, The Netherlands: Springer), 207–235.
- Doebelin, N., and Kleeberg, R. (2015). Profex: a graphical user interface for the Rietveld refinement program BGMN. *J. Appl. Crystallogr.* 48, 1573–1580. doi: 10.1107/S1600576715014685
- Ertani, A., Mietto, A., Borin, M., and Nardi, S. (2017). Chromium in agricultural soils and crops: a review. *Water Air Soil Pollut.* 228, 1–12. doi: 10.1007/S11270-017-3356-Y/FIGURES/3
- Flipkens, G., Blust, R., and Town, R. M. (2021). Deriving nickel (Ni(II)) and chromium (Cr(III)) based environmentally safe olivine guidelines for coastal enhanced silicate weathering. *Environ. Sci. Technol.* 55, 12362–12371. doi: 10.1021/ACS.EST.1C02974/ASSET/IMAGES/LARGE/ES1C02974\_0003.JPG
- Fuhr, M., Geilert, S., Schmidt, M., Liebetrau, V., Vogt, C., Ledwig, B., et al. (2022). Kinetics of olivine weathering in seawater: an experimental study. *Front. Climate* 4:831587. doi: 10.3389/fclim.2022.831587/BIBTEX
- Gbor, P. K., and Jia, C. Q. (2004). Critical evaluation of coupling particle size distribution with the shrinking core model. *Chem. Eng. Sci.* 59, 1979–1987. doi: 10.1016/J.CES.2004.01.047
- Gillman, G. P. (1980). The effect of crushed basalt scoria on the cation exchange properties of a highly weathered soil. *Soil Sci. Soc. Am. J.* 44, 465–468. doi: 10.2136/SSAJ1980.03615995004400030005X
- Gislason, S. R., Arnorsson, S., and Armannsson, H. (1996). Chemical weathering of basalt in Southwest Iceland; effects of runoff, age of rocks and vegetative/glacial cover. *Am. J. Sci.* 296, 837–907. doi: 10.2475/ajs.296.8.837
- Goll, D. S., Ciais, P., Amann, T., Buermann, W., Chang, J., Eker, S., et al. (2021). Potential CO<sub>2</sub> removal from enhanced weathering by ecosystem responses to powdered rock. *Nat. Geosci.* 14, 545–549. doi: 10.1038/s41561-021-00798-x
- Hänen, M., Prigobbe, V., Storti, G., Seward, T. M., and Mazzotti, M. (2006). Dissolution kinetics of festeritic olivine at 90–150°C including effects of the presence of CO<sub>2</sub>. *Geochim. Cosmochim. Acta* 70, 4403–4416. doi: 10.1016/j.gca.2006.06.1560
- Hangx, S. J. T., and Spiers, C. J. (2009). Coastal spreading of olivine to control atmospheric CO<sub>2</sub> concentrations: a critical analysis of viability. *Int. J. Greenhouse Gas Control* 3, 757–767. doi: 10.1016/j.ijggc.2009.07.001
- Haque, F., Chiang, Y. W., and Santos, R. M. (2020). Risk assessment of Ni, Cr, and Si release from alkaline minerals during enhanced weathering. *Open Agric* 5, 166–175. doi: 10.1515/OPAG-2020-0016/DOWNLOADASSET/SUPPL/OPAG-2020-0016\_SM.PDF
- Hartmann, J., Jansen, N., Dürr, H. H., Kempe, S., and Köhler, P. (2009). Global CO<sub>2</sub>-consumption by chemical weathering: what is the contribution of highly active weathering regions? *Glob. Planet. Chang.* 69, 185–194. doi: 10.1016/j.gloplacha.2009.07.007
- Hartmann, J., and Moosdorf, N. (2011). Chemical weathering rates of silicate-dominated lithological classes and associated liberation rates of phosphorus on the Japanese archipelago-implications for global scale analysis. *Chem. Geol.* 287, 125–157. doi: 10.1016/j.chemgeo.2010.12.004
- Hartmann, J., West, A. J., Renforth, P., Köhler, P., de La Rocha, C. L., Wolf-Gladrow, D. A., et al. (2013). Enhanced chemical weathering as a geoengineering strategy to reduce atmospheric carbon dioxide, supply nutrients, and mitigate ocean acidification. *Rev. Geophys.* 51, 113–149. doi: 10.1002/rog.20004
- Hatton, J. E., Hendry, K. R., Hawkings, J. R., Wadham, J. L., Kohler, T. J., Stibal, M., et al. (2019). Investigation of subglacial weathering under the Greenland ice sheet using silicon isotopes. *Geochim. Cosmochim. Acta* 247, 191–206. doi: 10.1016/j.chemgeo.2018.12.033
- Hellmann, R., Wirth, R., Daval, D., Barnes, J.-P., Penisson, J.-M., Tisserand, D., et al. (2012). Unifying natural and laboratory chemical weathering with interfacial dissolution-reprecipitation: a study based on the nanometer-scale chemistry of fluid-silicate interfaces. *Chem. Geol.* 294–295, 203–216. doi: 10.1016/j.chemgeo.2011.12.002
- IPCC (2021). “Summary For Policymakers,” In *Climate Change 2021: The Physical Science Basis. Contribution of Working Group I to the Sixth Assessment Report of the Intergovernmental Panel on Climate Change*, eds. V. Masson-Delmotte, P. Zhai, A. Pirani, S. L. Connors, C. Péan, S. Berger, et al. (Cambridge, United Kingdom and New York, NY, USA: Cambridge University Press), 3–32.
- IPCC (2022). *Global warming of 1.5°C: IPCC special report on impacts of global warming of 1.5°C above pre-industrial levels in context of strengthening response to climate change, sustainable development, and efforts to eradicate poverty*. 1st Edn Cambridge University Press.
- Kasting, J. F. (2019). The goldilocks planet? How silicate weathering maintains earth just right. *Elements* 15, 235–240. doi: 10.2138/gselements.15.4.235
- Köhler, P., Hartmann, J., and Wolf-Gladrow, D. A. (2010). Geoengineering potential of artificially enhanced silicate weathering of olivine. *Proc. Natl. Acad. Sci. USA* 107, 20228–20233. doi: 10.1073/pnas.1000545107
- Lembrechts, J. J., Hoogen, J., Aalto, J., Ashcroft, M. B., De Frenne, P., Kemppinen, J., et al. (2022). Global maps of soil temperature. *Glob. Chang. Biol.* 28, 3110–3144. doi: 10.1111/gcb.16060
- Lewis, J. F., Draper, G., Proenza, J. A., Espaillat, J., and Jiménez, J. (2006). Ophiolite-related ultramafic rocks (serpentinites) in the Caribbean region: a review of their occurrence, composition, origin, emplacement and Nilareite soil formation. *Geologica Acta: Int. Earth Sci.* J. 4, 237–263.
- Maher, K., Johnson, N. C., Jackson, A., Lammers, L. N., Torchinsky, A. B., Weaver, K. L., et al. (2016). A spatially resolved surface kinetic model for forsterite dissolution. *Geochim. Cosmochim. Acta* 174, 313–334. doi: 10.1016/j.gca.2015.11.019
- Manning, D. A. C., Renforth, P., Lopez-Capel, E., Robertson, S., and Ghazireh, N. (2013). Carbonate precipitation in artificial soils produced from basaltic quarry fines and composts: an opportunity for passive carbon sequestration. *Int. J. Greenhouse Gas Control* 17, 309–317. doi: 10.1016/j.ijggc.2013.05.012
- Meybeck, M. (1987). Global chemical weathering of surficial rocks estimated from river dissolved loads. *Am. J. Sci.* 287, 401–428. doi: 10.2475/ajs.287.5.401
- Oelkers, E. H., Declercq, J., Saldi, G. D., Gislason, S. R., and Schott, J. (2018). Olivine dissolution rates: a critical review. *Chem. Geol.* 500, 1–19. doi: 10.1016/j.chemgeo.2018.10.008
- Oelkers, E. H., Butcher, R., Pogge von Strandmann, P. A. E., Schüssler, J. A., von Blanckenburg, F., Snæbjörnsdóttir, S., et al. (2019). Using stable Mg isotope signatures to assess the fate of magnesium during the in situ mineralisation of CO<sub>2</sub> and H<sub>2</sub>S at the CarbFix site in SW-Iceland. *Geochimica et Cosmochimica Acta* 245, 542–555. doi: 10.1016/j.gca.2018.11.011
- Opfergelt, S., Burton, K. W., Georg, R. B., West, A. J., Guicharnaud, R. A., Sigfusson, B., et al. (2014). Magnesium retention on the soil exchange complex controlling mg isotope variations in soils, soil solutions and vegetation in volcanic soils, Iceland. *Geochim. Cosmochim. Acta* 125, 110–130. doi: 10.1016/j.gca.2013.09.036
- Parkhurst, D. L., and Appelo, C. A. J. (2013). Description of input and examples for PHREEQC version 3 -- a computer program for speciation, batch-reaction, one-dimensional transport, and inverse geochemical calculations. *US geological survey techniques and methods*, 6:497.
- Peters, S. C., Blum, J. D., Driscoll, C. T., and Likens, G. E. (2004). Dissolution of wollastonite during the experimental manipulation of Hubbard brook watershed 1. *Biogeochemistry* 67, 309–329. doi: 10.1023/B:BIOG.000015787.44175.3f
- Pogge von Strandmann, P. A. E., Burton, K. W., Opfergelt, S., Eiríksdóttir, E. S., Murphy, M. J., Einarsson, A., et al. (2016). The effect of hydrothermal spring weathering processes and primary productivity on lithium isotopes: Lake Myvatn, Iceland. *Chem. Geol.* 445, 4–13. doi: 10.1016/j.chemgeo.2016.02.026
- Pogge von Strandmann, P. A. E., Fraser, W. T., Hammond, S. J., Tarbuck, G., Wood, I. G., Oelkers, E. H., et al. (2019). Experimental determination of Li isotope behaviour during basalt weathering. *Chem. Geol.* 517, 34–43. doi: 10.1016/j.chemgeo.2019.04.020
- Pogge von Strandmann, P. A. E., Renforth, P., West, A. J., Murphy, M. J., Luu, T.-H., and Henderson, G. M. (2021). The lithium and magnesium isotope signature of olivine dissolution in soil experiments. *Chem. Geol.* 560:120008. doi: 10.1016/j.chemgeo.2020.120008
- Pogge von Strandmann, P. A. E., Tooley, C., Mulders, J. J. P. A., and Renforth, P. (2022). The dissolution of olivine added to soil at 4°C: implications for enhanced weathering in cold regions. *Front. Climate* 4:827698. doi: 10.3389/fclim.2022.827698
- Pogge von Strandmann, P. A. E., Vaks, A., Bar-Matthews, M., Ayalon, A., Jacob, E., and Henderson, G. M. (2017). Lithium isotopes in speleothems: temperature-controlled variation in silicate weathering during glacial cycles. *Earth Planet. Sci. Lett.* 469, 64–74. doi: 10.1016/j.epsl.2017.04.014
- Pokrovsky, O. S., and Schott, J. (2000). Kinetics and mechanism of forsterite dissolution at 25°C and pH from 1 to 12. *Geochim. Cosmochim. Acta* 64, 3313–3325. doi: 10.1016/S0016-7037(00)00434-8
- Powell, J. H., and Riding, J. B. (2016). Stratigraphy, sedimentology and structure of the Jurassic (Callovian to lower Oxfordian) succession at Castle Hill, Scarborough, North Yorkshire, UK. *Proc. Yorks. Geol. Soc.* 61, 109–133. doi: 10.1144/PYGS2016-365

- Psarras, P., Krutka, H., Fajardi, M., Zhang, Z., Liguori, S., Dowell, N. M., et al. (2017). Slicing the pie: how big could carbon dioxide removal be?: slicing the pie. *Wiley Interdiscip Rev Energy Environ* 6:e253. doi: 10.1002/wene.253
- Raveh-Rubin, S., Edery, Y., Dror, I., and Berkowitz, B. (2015). Nickel migration and retention dynamics in natural soil columns. *Water Resour. Res.* 51, 7702–7722. doi: 10.1002/2015WR016913
- Raymo, M. E., and Ruddiman, W. F. (1992). Tectonic forcing of late Cenozoic climate. *Nature* 359, 117–122. doi: 10.1038/359117a0
- Renforth, P. (2012). The potential of enhanced weathering in the UK. *Int. J. Greenhouse Gas Control* 10, 229–243. doi: 10.1016/j.ijgac.2012.06.011
- Renforth, P., and Henderson, G. (2017). Assessing Ocean alkalinity for carbon sequestration. *Rev. Geophys.* 55, 636–674. doi: 10.1002/2016RG000533
- Renforth, P., Jenkins, B. G., and Kruger, T. (2013). Engineering challenges of ocean liming. *Energy* 60, 442–452. doi: 10.1016/j.energy.2013.08.006
- Renforth, P., von Strandmann, P. A. E., and Henderson, G. M. (2015). The dissolution of olivine added to soil: implications for enhanced weathering. *Appl. Geochem.* 61, 109–118. doi: 10.1016/j.apgeochem.2015.05.016
- Rigopoulos, I., Harrison, A. L., Delimitis, A., Ioannou, I., Efstratiou, A. M., Kyratsi, T., et al. (2018). Carbon sequestration via enhanced weathering of peridotites and basalts in seawater. *Appl. Geochem.* 91, 197–207. doi: 10.1016/J.APGEOCHEM.2017.11.001
- Rockström, J., Gaffney, O., Rogelj, J., Meinshausen, M., Nakicenovic, N., and Schellnhuber, H. J. (2017). A roadmap for rapid decarbonization. *Science* 355, 1269–1271. doi: 10.1126/science.aah3443
- Saenger, C., and Wang, Z. (2014). Magnesium isotope fractionation in biogenic and abiogenic carbonates: implications for paleoenvironmental proxies. *Quat. Sci. Rev.* 90, 1–21. doi: 10.1016/J.QUASCIREV.2014.01.014
- Schaller, J., Puppe, D., Kaczorek, D., Ellerbrock, R., and Sommer, M. (2021). Silicon cycling in soils revisited. *Plant. Theory* 10:295. doi: 10.3390/plants10020295
- Schopka, H. H., Derry, L. A., and Arcilla, C. A. (2011). Chemical weathering, river geochemistry and atmospheric carbon fluxes from volcanic and ultramafic regions on Luzon Island, the Philippines. *Geochim. Cosmochim. Acta* 75, 978–1002. doi: 10.1016/j.gca.2010.11.014
- Schuiling, R. D., and de Boer, P. L. (2010). Coastal spreading of olivine to control atmospheric CO<sub>2</sub> concentrations: a critical analysis of viability. Comment: nature and laboratory models are different. *Int. J. Greenhouse Gas Control* 4, 855–856. doi: 10.1016/j.ijgac.2010.04.012
- Schuiling, R. D., and Krijgsman, P. (2006). Enhanced weathering: an effective and cheap tool to sequester CO<sub>2</sub>. *Clim. Chang.* 74, 349–354. doi: 10.1007/s10584-005-3485-y
- Song, Z., Liu, C., Müller, K., Yang, X., Wu, Y., and Wang, H. (2018). Silicon regulation of soil organic carbon stabilization and its potential to mitigate climate change.
- Stefansson, A. (2001). Chemical weathering of basalts, Southwest Iceland: effect of rock crystallinity and secondary minerals on chemical fluxes to the ocean. *Am. J. Sci.* 301, 513–556. doi: 10.2475/ajs.301.6.513
- Strelfer, J., Amann, T., Bauer, N., Kriegler, E., and Hartmann, J. (2018). Potential and costs of carbon dioxide removal by enhanced weathering of rocks. *Environ. Res. Lett.* 13:34010. doi: 10.1088/1748-9326/aa9c4
- Suchet, P. A., and Probst, J. L. (1995). A global model for present-day atmospheric/soil CO<sub>2</sub> consumption by chemical erosion of continental rocks (GEM-CO<sub>2</sub>). *Tellus B* 47, 273–280. doi: 10.1034/j.1600-0889.47.issue1.23.x
- Taylor, L. L., Quirk, J., Thorley, R. M. S., Kharecha, P. A., Hansen, J., Ridgwell, A., et al. (2016). Enhanced weathering strategies for stabilizing climate and averting ocean acidification. *Nat. Clim. Chang.* 6, 402–406. doi: 10.1038/nclimate2882
- Te Pas, E. E. E. M., Hagens, M., and Comans, R. N. J. (2023). Assessment of the enhanced weathering potential of different silicate minerals to improve soil quality and sequester CO<sub>2</sub>. *Front. Climate* 4. doi: 10.3389/fclim.2022.954064
- ten Berge, H. F. M., van der Meer, H. G., Steenhuijen, J. W., Goedhart, P. W., Knops, P., and Verhagen, J. (2012). Olivine weathering in soil, and its effects on growth and nutrient uptake in ryegrass (*Lolium perenne* L.): a pot experiment. *PLoS One* 7:e42098. doi: 10.1371/journal.pone.0042098
- Tessier, A., Campbell, P. G. C., and Bisson, M. (1979). Sequential extraction procedure for the speciation of particulate trace metals. *Anal. Chem.* 51, 844–851. doi: 10.1021/AC50043A017
- Tipper, E. T., Stevenson, E. I., Alcock, V., Knight, A. C. G., Baronas, J. J., Hilton, R. G., et al. (2021). Global silicate weathering flux overestimated because of sediment–water cation exchange. *Proc. Natl. Acad. Sci.* 118. doi: 10.1073/pnas.2016430118
- UNFCCC (2015). *Adoption of the Paris Agreement, 21st Conference of the Parties*. Paris: United Nations.
- Verbruggen, E., Struyf, E., and Vicca, S. (2021). Can arbuscular mycorrhizal fungi speed up carbon sequestration by enhanced weathering? *Plants, People, Planet* 3, 445–453. doi: 10.1002/PPP3.10179
- Versteegh, E. A. A., Black, S., and Hodson, M. E. (2014). Environmental controls on the production of calcium carbonate by earthworms. *Soil Biol. Biochem.* 70, 159–161. doi: 10.1016/j.soilbio.2013.12.013
- Vicca, S., Goll, D. S., Hagens, M., Hartmann, J., Janssens, I. A., Neubeck, A., et al. (2022). Is the climate change mitigation effect of enhanced silicate weathering governed by biological processes? *Glob. Chang. Biol.* 28, 711–726. doi: 10.1111/GCB.15993
- Vienne, A., Frings, P., Poblador, S., Steinwidder, L., Rijnders, J., Schoelynck, J., et al. (2023). Soil carbon sequestration and the role of earthworms in an enhanced weathering Mesocosm experiment. *SSRN* 4449286. doi: 10.2139/ssrn.4449286
- Voet, E. V., Salmine, R., Eckelman, M., Mudd, G., Norgate, T., and Hisscher, R. (2013). *Environmental risks and challenges of anthropogenic metals flows and cycles, a report of the working group on the global metal flows to the international resource panel* (Doctoral dissertation, Leiden).
- Wada, K., and Harada, Y. (1971). Effects of temperature on the measured cation-exchange capacities of ando soils. *J. Soil Sci.* 22, 109–117. doi: 10.1111/j.1365-2389.1971.tb01598.x
- Walker, J. C. G., Hays, P. B., and Kasting, J. F. (1981). A negative feedback mechanism for the long-term stabilization of Earth's surface temperature. *J. Geophys. Res.* 86, 9776–9782. doi: 10.1029/JC086iC10p09776
- West, L. J., Banwart, S. A., Martin, M. V., Kantzas, E., and Beerling, D. J. (2023). Making mistakes in estimating the CO<sub>2</sub> sequestration potential of UK croplands with enhanced weathering. *Appl. Geochem.* 151:105591. doi: 10.1016/j.apgeochem.2023.105591
- West, A., Galy, A., and Bickle, M. (2005). Tectonic and climatic controls on silicate weathering. *Earth Planet. Sci. Lett.* 235, 211–228. doi: 10.1016/j.epsl.2005.03.020
- Weyl, P. K. (1959). The change in solubility of calcium carbonate with temperature and carbon dioxide content. *GeCoA* 17, 214–225. doi: 10.1016/0016-7037(59)90096-1
- White, A. F., and Brantley, S. L. (2003). The effect of time on the weathering of silicate minerals: why do weathering rates differ in the laboratory and field? *Chem. Geol.* 202, 479–506. doi: 10.1016/J.CHEMGEOL.2003.03.001
- Wimpenny, J., Gíslason, S. R., James, R. H., Gannoun, A., Pogge Von Strandmann, P. A. E., and Burton, K. W. (2010). The behaviour of Li and mg isotopes during primary phase dissolution and secondary mineral formation in basalt. *Geochim. Cosmochim. Acta* 74, 5259–5279. doi: 10.1016/j.gca.2010.06.028